3.5.4 ICRS Centre

The International Earth Rotation and Reference System (IERS) International Celestial Reference System (ICRS) Centre is tasked with the maintenance of the International Celestial Reference System (ICRS) and the International Celestial Reference Frame (ICRF) for the international astronomical and geodesy communities. Responsibilities are shared jointly between Paris Observatory (OP) and the U.S. Naval Observatory (USNO). Critical ICRS and ICRF-relevant activities from 2019 are described for both OP and USNO in the following sections.

Paris Observatory IERS ICRS Centre Activities During 2019–2020

The International Reference Frame ICRF3

Resolution B2 of the XXX IAU General Assembly (IAU 2019) resolves that as from 1 January 2019 ICRF3 is the fundamental realization of the International Celestial Reference System (ICRS). This third representation of the International Celestial Reference System (ICRS) in radio wavelengths is a catalog of radio source positions described in Charlot et al. (2020). The ICRF3 consists of three catalogs at bands S/X, K and X/Ka with 4536, 824 and 678 objects, respectively (http://iers.obspm.fr/icrs-pc/newwww/icrf). Objects in the new frame had been used to orient the second Gaia data release DR2 catalog onto the ICRS, as will be the case for the Gaia final catalog.

Monitoring of the ICRS

Monitoring the ICRS is a mission of the IERS ICRS Centre. This includes verifications of the stability of the axes of the system materialized though the frame, identification of the possible deformations of the frame and tracking the astrometric evolution of its defining sources. Another aspect of this activity consists of the analysis of individual solutions submitted by the VLBI analysis centers to the International VLBI Service for Geodesy and Astrometry (IVS). The IERS ICRS Centre at Paris Observatory developed the tools for determining the orientation of the axes, characterizing the deformations of the frame and analyzing the astrometric quality of radio source positions (Lambert 2014). For this report, analyses with respect to the conventional reference ICRF3 are presented, as well as with respect to Gaia DR2, which constitutes a preliminary version of the catalog that will allow access to the ICRS in optical wavelengths.

Analysis of Recent VLBI Catalogs

Data

We analyzed five catalogs submitted to the IVS in 2019. The catalogs were respectively submitted by the Space Geodesy Centre of the Italian Space Agency (ASI/CGS; solution asi2019a), by Geoscience Australia (aus2019a and 2019b), by Paris Observatory (opa2019a) and by the Unites States Naval Observatory (usn2019c). The two solutions aus2019a and aus2019b were obtained with the OCCAM geodetic VLBI analysis software package (Titov et al. 2004), whereas the other four catalogs were obtained with Calc/Solve (Ma et al. 1986). The catalogs were released after the date of adoption of the ICRF3; therefore, their individual frames had been oriented to ICRF3 by applying no net rotation constraints, with the exception of the ASI solution, which has been oriented to ICRF2 (Fey et al. 2015). Positions in ICRF3 had been adopted for the a priori catalogs in the solutions, with the exception of ASI, where the a priori source positions are the ICRF2 coordinates. In our analysis we have compared these individual solutions to the catalog representing ICRF3 in the S/X bands (ICRF3X in this report). The 2983 sources in common between the ICRF3 and the second Gaia data release (DR2; Prusti et al. 2016; Brown et al. 2016, 2018; Mignard et al. 2018) have been used also as a reference for comparison.

Overview of the Catalogs

The number of sources in each catalog, the mean epoch of the observations, and the median positional errors (for RA cos DEC, Dec, and for the error ellipse major axis) are reported in Table 1. The standard error of the catalog positions differs in the solutions; the smallest values from ASI may depend on the choice of very good sources, AUS positions might be influenced by a large number of sources with errors in the range 0.6 – 1 mas in the Southern hemisphere. The USN solution did not consider a number of “special” sessions including VCS sessions and provide therefore coordinates for a relatively small number of sources.

Table 1: *Statistic information of the catalogs here reported. N is the number of sources. The mean epoch corresponds to the average of the mean observational epochs of each source. N is the number of sources, e_RA*, e_Dec are respectively the median standard errors in right ascension (scaled by cos dec) and in declination, e_EEMA is the median major axis of error ellipses. Unit is μas.*

Catalog	N	Epoch	e_RA*	e_Dec	e_EEMA
opa2019	a4468	2010.93	116.90	196.55	205.89
aus2019	a4529	2012.71	261.57	478.00	496.19
aus2019	b4645	2012.96	273.72	471.20	493.59
asi2019	a3850	2013.78	74.98	130.80	133.37
usn2019	c2390	2012.01	171.77	259.80	289.09

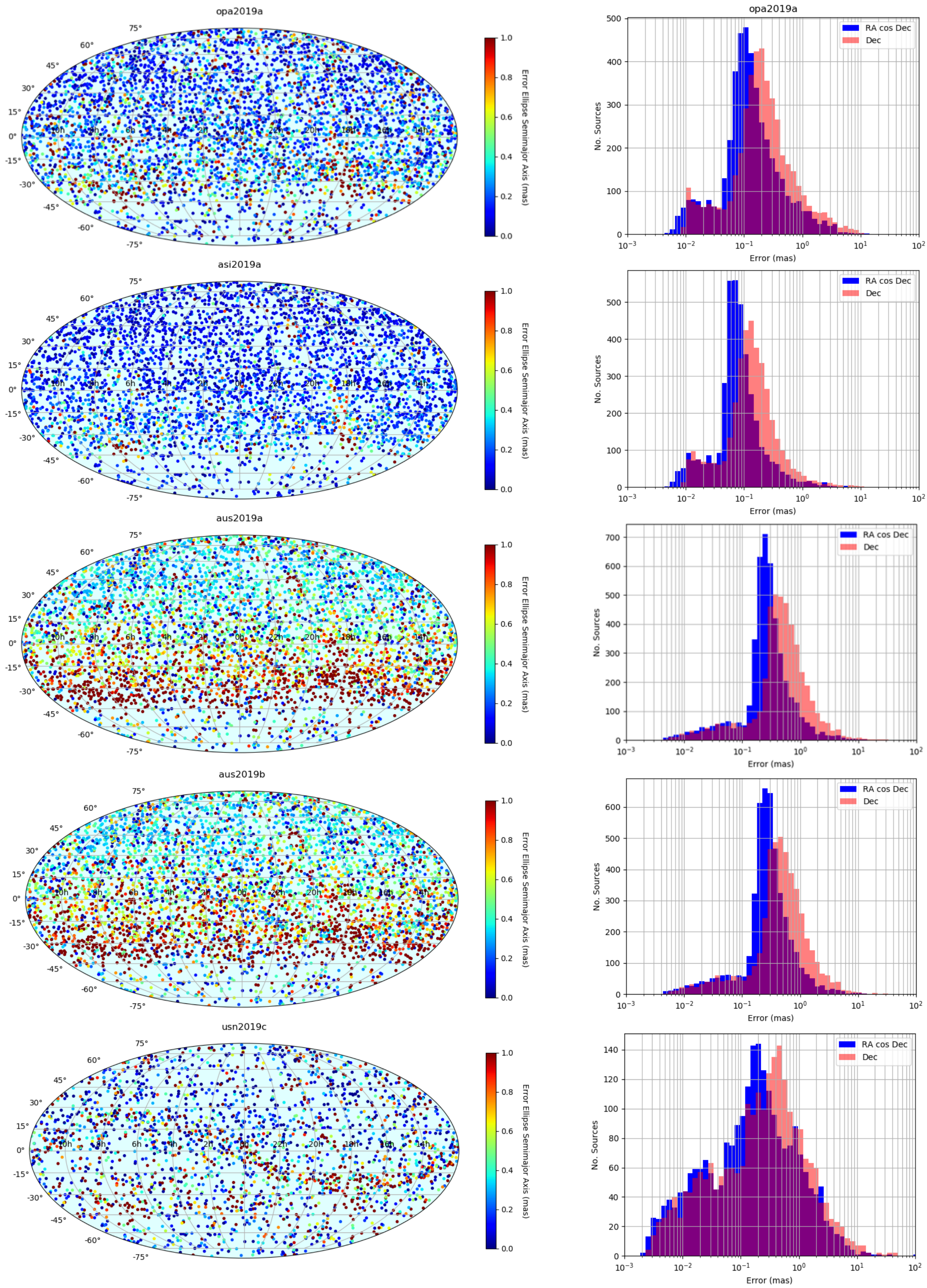

Fig. 1: *Left: sky distribution of the catalogs highlighting the overall positional error computed as the major axis of the error ellipse. Right: distribution of the standard errors on source position.*

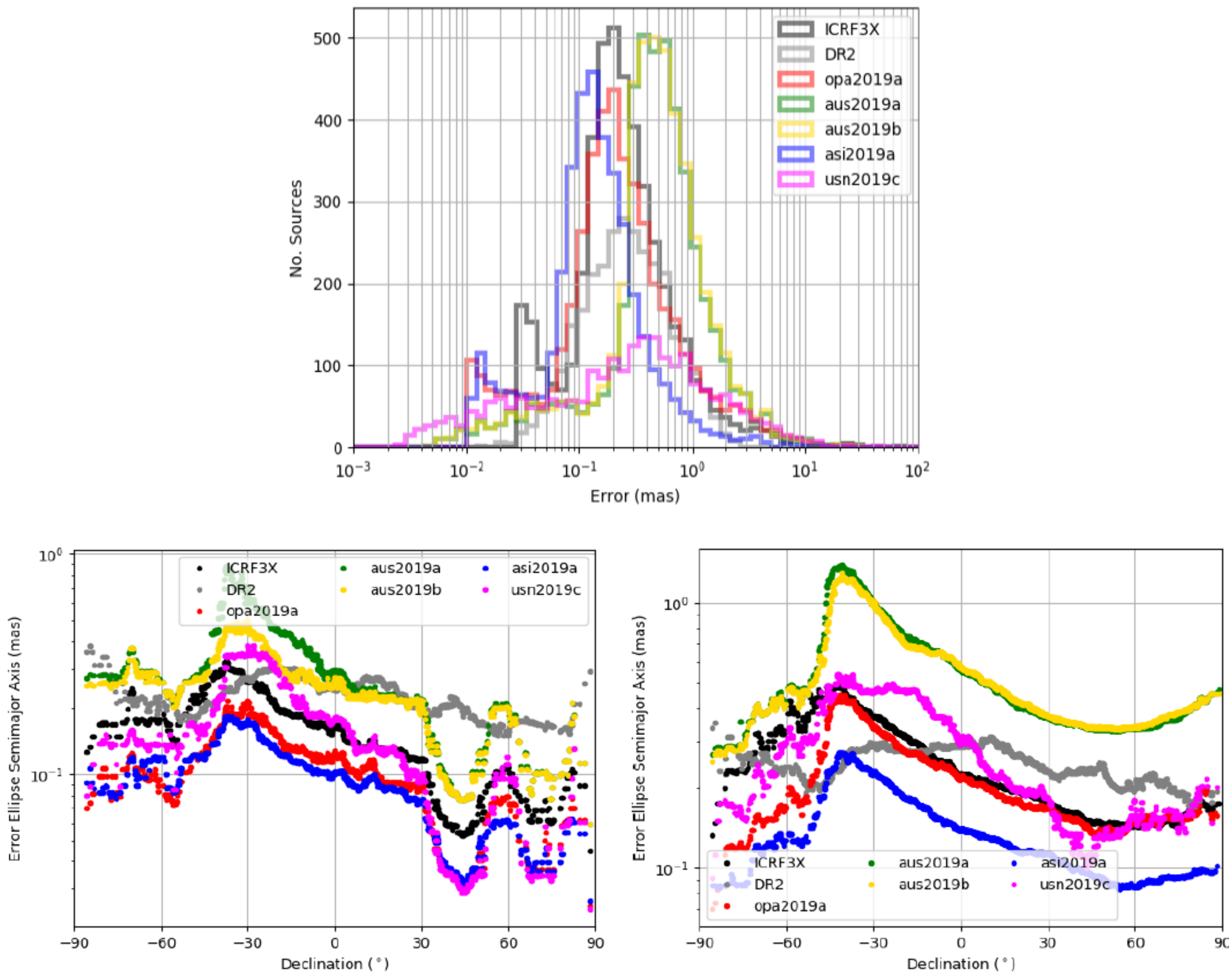

Fig. 2: *Top: overall comparison of the standard error distribution. Bottom: standard errors in source positions as a function of the declination smoothed by taking the running median within bins of 15 degrees, for sources common to all catalogs (left) and for all sources in each catalog (right).*

The sky distribution of the radio sources in each catalog is plotted in Figure 1 together with the distribution of the standard errors. In the sky maps, the color indicates the overall error computed as the major axis of the error ellipse, calculated using the correlation information between the coordinates as provided in the catalogs. Figure 2 presents three plots; on top the error distribution, including that of the catalogs used as reference in the comparisons (ICRF3X and Gaia DR2); at the bottom the dependence of the error on the declination including the common sources to all catalogs (left) and all sources in each catalog (right) are displayed for which we took the running median error within windows of 15°. The plots show a clear declination-dependent error for the individual catalogs. When sources common to all catalogs are considered, the behavior of the VLBI solutions is similar, peaking at about -30° declination, and reaching small error values around +45° declination, certainly due to the presence of a substantial number of good astrometric common sources in that region. This effect is not visible in the plot where all sources in each catalog are considered. Both AUS solutions show the largest errors, particularly at mid-latitudes in the Southern hemisphere, very probably due to the network asymmetry and the quality of the sources in the South, visible in the plots of Fig. 1. The Gaia scanning law allows to cover both hemispheres symmetrically, and in consequence the Gaia DR2 catalog does not show such systematic effects.

Comparison with ICRF3 and Gaia DR2

Figure 3 displays the differences in declination between the catalogs and the references averaged within bins of 200 sources in two configurations: all sources (left) and sources common to all catalogs (right).

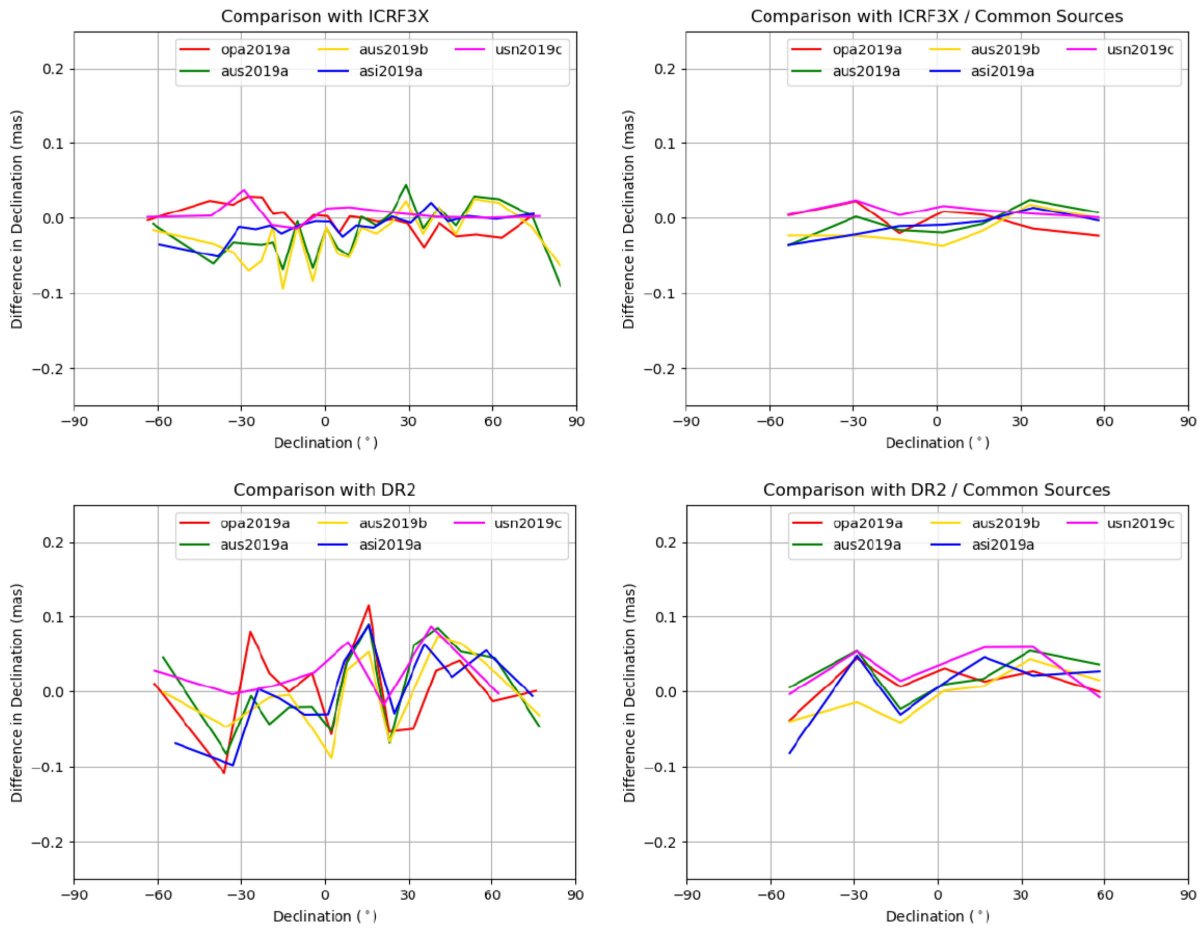

Fig. 3: *Differences in declination between the catalogs and the references (ICRF3X: top; Gaia DR2, bottom) averaged in bins of 200 sources sorted by declination for all sources (left) and for common sources to all catalogs (right).*

Most deformations are smaller than 50 μas when the differences with respect ICRF3X are computed with all the sources in each catalog (top left), only the AUS solutions present effects close to 0.1 mas between

0° and -30°, probably due to the network geometry and the quality of sources at negative declinations. Deformations are smoother when the differences are computed with common sources (top right), they remain within less than 40 μas. The amplitude of the deformations is bigger when the differences are computed with respect to Gaia DR2, since the sphere of Gaia is in principle not affected by deformations.

Catalog comparisons had been computed using the 16-parameter transformation accounting for rotations around the three axes, a glide, and degree-2 electric- and magnetic-type deformations (see e.g., Mignard and Klioner 2012). The coordinate differences $\Delta\alpha$ and $\Delta\delta$ between a catalog and a reference catalog read:

$$\begin{aligned}
\Delta\alpha\cos\delta &= R_1\cos\alpha\sin\delta + R_2\sin\alpha\sin\delta - R_3\cos\delta - D_1\sin\alpha + D_2\cos\alpha + M_{20}\sin 2\delta \\
&+ \left(E_{21}^{\mathrm{Re}}\sin\alpha + E_{21}^{\mathrm{Im}}\cos\alpha\right)\sin\delta - \left(M_{21}^{\mathrm{Re}}\cos\alpha - M_{21}^{\mathrm{Im}}\sin\alpha\right)\cos 2\delta \\
&- 2\left(E_{22}^{\mathrm{Re}}\sin 2\alpha + E_{22}^{\mathrm{Im}}\cos 2\alpha\right)\cos\delta - \left(M_{22}^{\mathrm{Re}}\cos 2\alpha - M_{22}^{\mathrm{Im}}\sin 2\alpha\right)\sin 2\delta, \\
\Delta\delta &= -R_1\sin\alpha + R_2\cos\alpha - D_1\cos\alpha\sin\delta - D_2\sin\alpha\sin\delta + D_3\cos\delta + E_{20}\sin 2\delta \\
&- \left(E_{21}^{\mathrm{Re}}\cos\alpha - E_{21}^{\mathrm{Im}}\sin\alpha\right)\cos 2\delta - \left(M_{21}^{\mathrm{Re}}\sin\alpha + M_{21}^{\mathrm{Im}}\cos\alpha\right)\sin\delta \\
&- \left(E_{22}^{\mathrm{Re}}\cos 2\alpha - E_{22}^{\mathrm{Im}}\sin 2\alpha\right)\sin 2\delta + 2\left(M_{22}^{\mathrm{Re}}\sin 2\alpha + M_{22}^{\mathrm{Im}}\cos 2\alpha\right)\cos\delta,
\end{aligned}$$

where α and δ are the coordinates of the object in the reference catalog. We used weighted least-squares to solve the system, with weights computed using the available covariance information (i.e., the standard errors on individual source coordinates and their correlation). The values of the transformation parameters adjusted to the catalogs compared to the ICRF3X and Gaia DR2 and their standard errors are reported in Figure 4 for two different set of sources, those common to all catalogs and each reference, and those common between each catalog and the reference. The resulting statistics after removal of systematics are reported in Table 2. Fig. 4 reveals that the results are similar independently from the set of sources used for the comparisons. The comparisons with ICRF3X show rotations of about 50 μas around the x and y axes for the OP and ASI solutions, and no significant deformations in all cases. Gaia DR2 has been oriented onto ICRF3, and we could expect no significant rotation between its axes and the VLBI solutions; this is the case, since the significant rotations in the plot correspond to the OP and ASI solutions, rotated with respect to ICRF3X. Deformations are visibly dependent on declination, consistent with Figure 2.

Table 2: *Statistics of the differences of the catalogs to ICRF3X and Gaia DR2 with different sets of common sources, and after removal of large-scale systematics. RA* stands for RA cos_dec. Unit is μas.*

a. With respect to ICRF3X, N: number of sources common to ICRF3X and each individual catalog.

Catalog	N	Std_RA*	Std_Dec	Chi2_RA*	Chi2_Dec	Std_RA*	Std_Dec	Chi2_RA*	Chi2_Dec
opa2019a	4381	76.52	92.83	0.71	0.75	73.31	82.92	0.65	0.6
aus2019a	4433	107.19	122.07	0.83	0.83	106.91	121.4	0.83	0.82
aus2019b	4434	110.68	121.56	0.9	0.84	109.92	120.55	0.88	0.82
asi2019a	3799	69	84.52	0.68	0.71	66.05	75.36	0.62	0.57
usn2019c	2274	62.83	63.88	0.81	0.68	62.74	63.61	0.81	0.67

b. With respect to ICRF3X, N: number of sources common to all catalogs.

Catalog	N	Std_RA*	Std_Dec	Chi2_RA*	Chi2_Dec	Std_RA*	Std_Dec	Chi2_RA*	Chi2_Dec
opa2019a	1375	50.55	66.06	0.67	0.89	45.79	51.35	0.55	0.54
aus2019a	1379	69.7	75.32	0.9	0.87	69.21	74.37	0.89	0.85
aus2019b	1379	71.81	75.92	0.97	0.9	70.77	74.4	0.94	0.86
asi2019a	1375	53.85	65.4	0.76	0.85	49.81	53	0.65	0.56
usn2019c	1375	53.9	54.19	0.77	0.63	53.79	53.9	0.76	0.62

c. With respect to Gaia-DR2, N: number of sources common to DR2 and each individual catalog.

Catalog	N	Std_RA*	Std_Dec	Chi2_RA*	Chi2_Dec	Std_RA*	Std_Dec	Chi2_RA*	Chi2_Dec
opa2019a	2912	301.75	316.07	2.44	2.37	298.93	311.05	2.39	2.3
aus2019a	2920	354.26	355.35	2.1	1.73	352.41	353.16	2.08	1.71
aus2019b	2920	356.79	353.53	2.14	1.76	354.8	350.8	2.12	1.73
asi2019a	2525	263.54	286.96	2.41	2.48	262.29	283.17	2.39	2.41
usn2019c	1596	262.69	263.91	2.3	2.27	260.82	262.14	2.27	2.24

d. With respect to Gaia-DR2, N: number of sources common to all catalogs.

Catalog	N	Std_RA*	Std_Dec	Chi2_RA*	Chi2_Dec	Std_RA*	Std_Dec	Chi2_RA*	Chi2_Dec
opa2019a	1375	261.61	262.76	2.54	2.56	258.68	256.66	2.49	2.45
aus2019a	1379	291.64	285.37	2.36	2.09	288.84	281.43	2.31	2.04
aus2019b	1379	288.29	287.63	2.35	2.2	285.41	282.94	2.3	2.13
asi2019a	1375	245.37	253.55	2.45	2.49	243.96	248.34	2.43	2.38

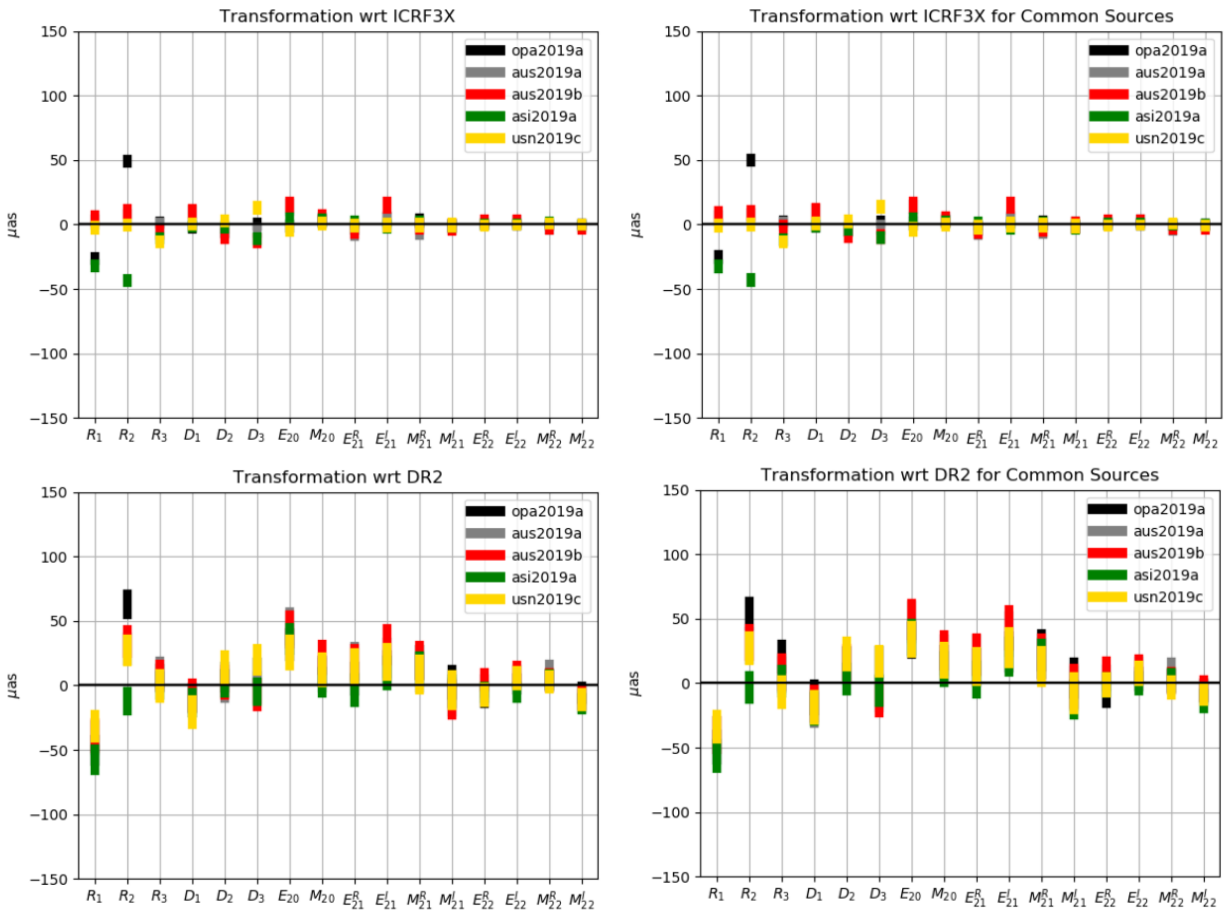

Fig. 4: *Transformation parameters between the catalogs under analysis and the reference frames (ICRF3X: top, Gaia DR2: bottom). The plots on the left represent parameters computed with sources common to each individual catalog and the frame used as reference (from top to bottom they correspond to the statistics in Tables 2a and 2c); the plots on the right represent parameters computed with sources common to all the catalogs involved in the comparisons, including the references (from top to bottom they correspond to the statistics in Tables 2b and 2d).*

Galactic aberration has been accounted for at the construction of ICRF3. Uncorrected Galactic aberration should provoke a glide of amplitude close to 5 μas/yr (e.g., Kovalevsky 2003; Titov et al. 2011) towards the Galactic center (approx. R.A. 265° and declination -29°). A value of 5.8 μas/yr for the amplitude of the Galactic aberration has been evaluated in analyses performed at the construction of the ICRF3 (MacMillan et al. 2019). The descriptions of the solutions provided to the IVS used in this report indicate that this correction has been applied in the OP, AUS, and USN solutions (for details refer to http://ivsopar.obspm.fr/vlbi/ivsproducts/crf/). The effect of uncorrected Galactic aberration in the ASI solution is not clearly visible in the deformation parameters since the mean epochs of the catalogs are close to that of ICRF3 (2015.0) and Gaia DR2 (2015.5).

Conclusions and recommendations

Five individual catalogs submitted to the IVS in 2019 are analyzed in this report. The axes of their frames are consistent with ICRF3X at the level of 50 μas without any zonal deformation beyond 15 μas. This result is also valid for the ASI solution, which has been aligned to ICRF2, confirming the good consistency between ICRF2 and ICRF3. Compared to Gaia DR2, a similar misalignment, of order 50 μas is visible, with significant zonal deformations particularly for the AUS solutions.

For a better evaluation of the consistency of the VLBI products and a better maintenance of the reference frame, we request analysis centers submit solutions aligned to the new reference ICRF3, as well as to adopt the ICRF3 catalogue for the a priori positions in the solutions. In all solutions the correction for the amplitude of the Galactic aberration must be implemented using the recommended value. These catalogs should be as complete as possible, i.e., processing as many VLBI sessions as possible since 1979. Analysis strategies should be rigorously documented and motivated. The main points that will be scrutinized in the next reports will be the zonal systematics, their relation with the Galactic aberration, and the agreement with the current (DR2) and future releases of Gaia.

Photometric follow-up of ICRF quasars

During the year 2019 the funding dossier creation phase for the 1m telescope dedicated to the photometry of active galactic nuclei (AGNs) was completed. The dossier was sent to the French DIM-ACAV financial support and accepted mid-2019. The funds obtained represent more or less one half of the total amount of necessary funds. A second independent funding request was then prepared and sent at the end of the year; results have yet to be received during 2020. This project was initiated in 2015 “ex nihilo” by the choice of the site and the demonstration of its quality (median value of the seeing is 1”, mode seeing is 0.7”). A feasibility phase to ensure the possibility to manage a remote instrument was then initiated and completed. The last phase will be the realization of the telescope and the implantation on site once the result for the second funding request is known. The heart of the scientific program of the telescope will be the monitoring of AGNs. Asteroid and exoplanet observations together with GRB optical counterpart follow up, and teaching, will be other tasks devoted to this instrument.

During 2019 the collaboration with Dr. Damljanovic (Belgrade Observatory) continued its program of observations of AGNs for the link between reference systems (magnitude monitoring). Another collaboration with USNO has been established during two meetings at Paris Observatory (FRAMEx project in February and October). The goal is to observe AGNs at various wavelengths (radio, infrared, optical, and X-ray) to better understand some significant radio-optical astrometric offsets.

Validation of the Gaia catalogue in the CU9

The main goal of the Gaia mission is to create an extraordinarily precise three-dimensional map of more than one billion objects (stars, asteroids, quasars) throughout our Galaxy and beyond. The Gaia mission through its successive releases delivers an astronomical catalogue and data archive of unprecedented scope, accuracy and completeness. A large pan-European team of expert scientists and software developers known as DPAC (Data Processing and Analysis Consortium) is responsible for the processing of Gaia's data with the final objective of producing the Gaia Catalogue. Coordinated by the DPAC Executive, the consortium is sub-divided into nine smaller, specialist units known as Coordination Units, or CUs, with each unit being assigned a unique set of data processing tasks.

Some members of the ICRS Centre belong to the CU9/WP944 group, responsible for validation of Gaia Catalogue Data Release with the validation Test Report. The aim of these tests is to check that Gaia data is coherent compared to other known catalogues, so as to accept or reject them for publication. In 2019, we have updated external catalogue files, tests code and reports to validate QSOs and AGNs included in the Gaia Catalogue Data Release DR3. These tests include rotation, cross-matching and completeness of these sources compared with QSO and AGN from external catalogues. The external catalogues used are ICRF3, LQAC5, GIQC, SDSS DR14Q, as well as specific catalogs as AGNs in Extended Sources Catalog where the probability for a QSO or AGN status is well defined.

Astrometric and Photometric Studies from the LQAC-5

One of the important tasks which the ICRS Centre is responsible for concerns the selection of the extragalactic sources that are likely to belong to the future generations of the ICRF. For that purpose, successive updates of the LQAC (Large Quasar Astrometric Catalogue) were constructed, including the LQAC-3 (Souchay et al. 2015) and the LQAC-4 (Gattano et al. 2018).

In 2019 we have published the fifth version of the LQAC, LQAC-5 (Souchay et al. 2019). It consists of a compilation of all the objects identified as quasars by the authors involved in the compilation of the catalogues, with criteria depending on each of these catalogues. In particular, new quasars from the SDSS DR14Q release (Pâris et al. 2018) were cross-matched with the previous LQAC-4 compilation, which lead to 149,084 new objects. Moreover, a great advantage with respect to this previous LQAC-4 version was the cross-match with the Gaia DR2 catalogue, which improved considerably the quality of astrometric data of the common objects. Furthermore, a precious new additional dataset was the inclusion of mid-infrared photometry from AllWISE (Wright et al. 2010). The LQAC-5 contains a total number of 592,809 quasars, which represent a 34% increase with respect to the number of objects recorded in the LQAC-4. Among them, 398,697 quasars were cross-matched with the Gaia DR2 catalogue, which correspond to 67% of the whole LQAC-5 population. Notice that in complement to original information such as multi-band photometry and redshifts directly obtained from the catalogues, we have provided in the LQAC-5 additional information such as morphology index and absolute magnitudes.

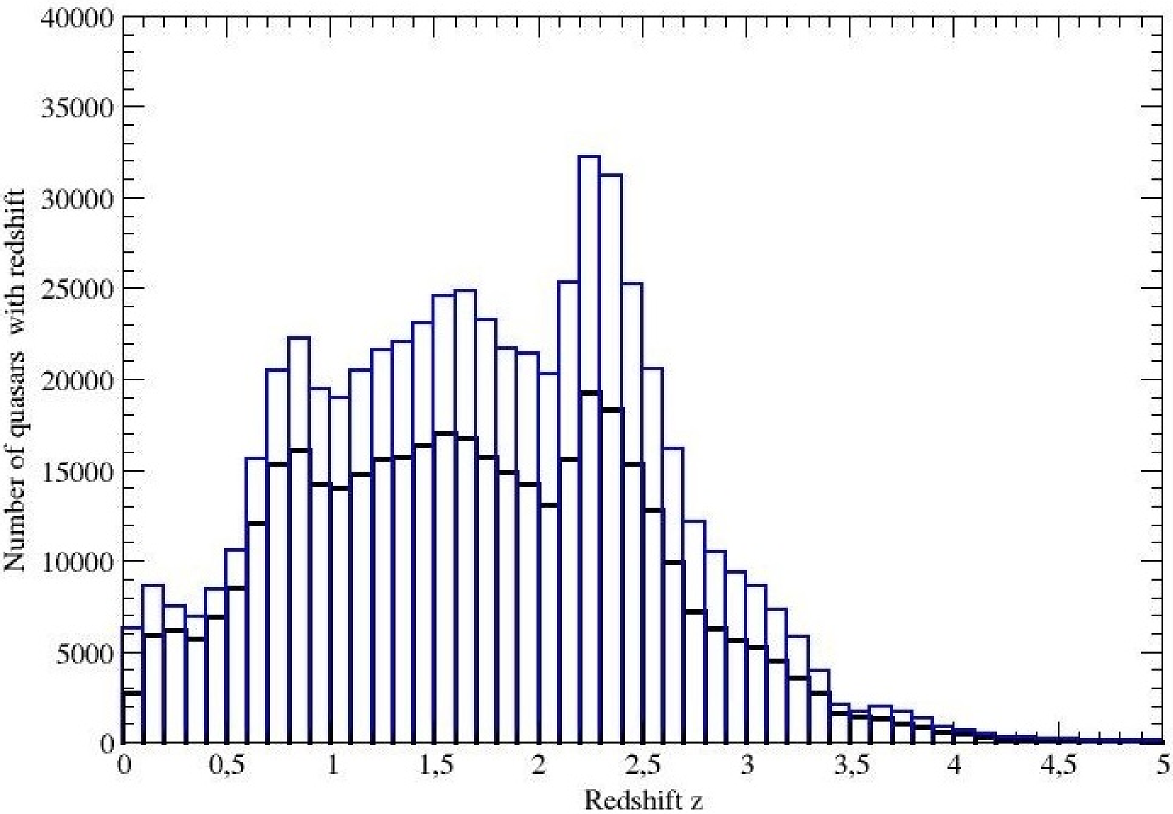

Fig. 5: *Redshift distribution of the whole LQAC-5 sample (blue) and of the Gaia DR2 sub-sample (black).*

In the following we give some interesting results related to the cross-match between the LQAC-5 and the Gaia DR2 catalogue. In particular, when it is possible, we compare our results with those of Mignard et al. (2018) who constructed what they called the Gaia CRF2, starting from a set of 566,869 AGNs still selected from mid-infrared color-color criteria. The important difference between these objects with respect to our LQAC-5 compilation lies in the fact that no redshift or related spectrum is available, so that they cannot be identified definitively as quasars. In Figure 5 we show the distribution of redshifts both for the whole LQAC-5 objects and for the objects in common with the DR2. We observe that the feature of both histograms is quite similar, in particular with the two peaks occurring respectively for z = 1.5 and z = 2.5. It means that the limitation of the LQAC-5 to the DR2 sub-sample does not affect significantly the redshift distribution.

In Figure 6 we show the cumulative histogram of the G magnitude of the common LQAC-5 – DR2 quasars. We remark that the number of quasars increases significantly in the interval 20 < G < 20.8 whereas it decreases considerably in the case of the CRF2.

We investigated the completeness of the Gaia DR2 catalogue with respect to the g magnitude of SDSS quasars belonging to the LQAC-5. Results are shown in Figure 7. We remark that all the quasars with g < 20.6 have been detected by Gaia, but that the number of objects with no Gaia counterpart increases steadily after this threshold to reach 30% at g = 21 and 80% at g = 21.7.

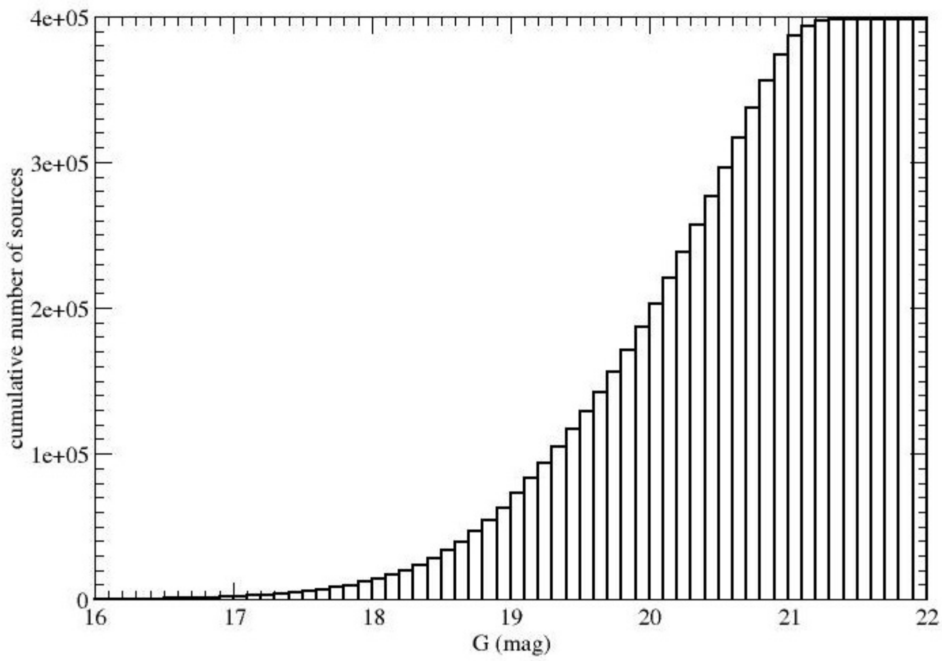

Fig. 6: *Cumulative distribution of the Gaia G magnitude of the LQAC-5 sub-sample of quasars cross-matched with Gaia DR2.*

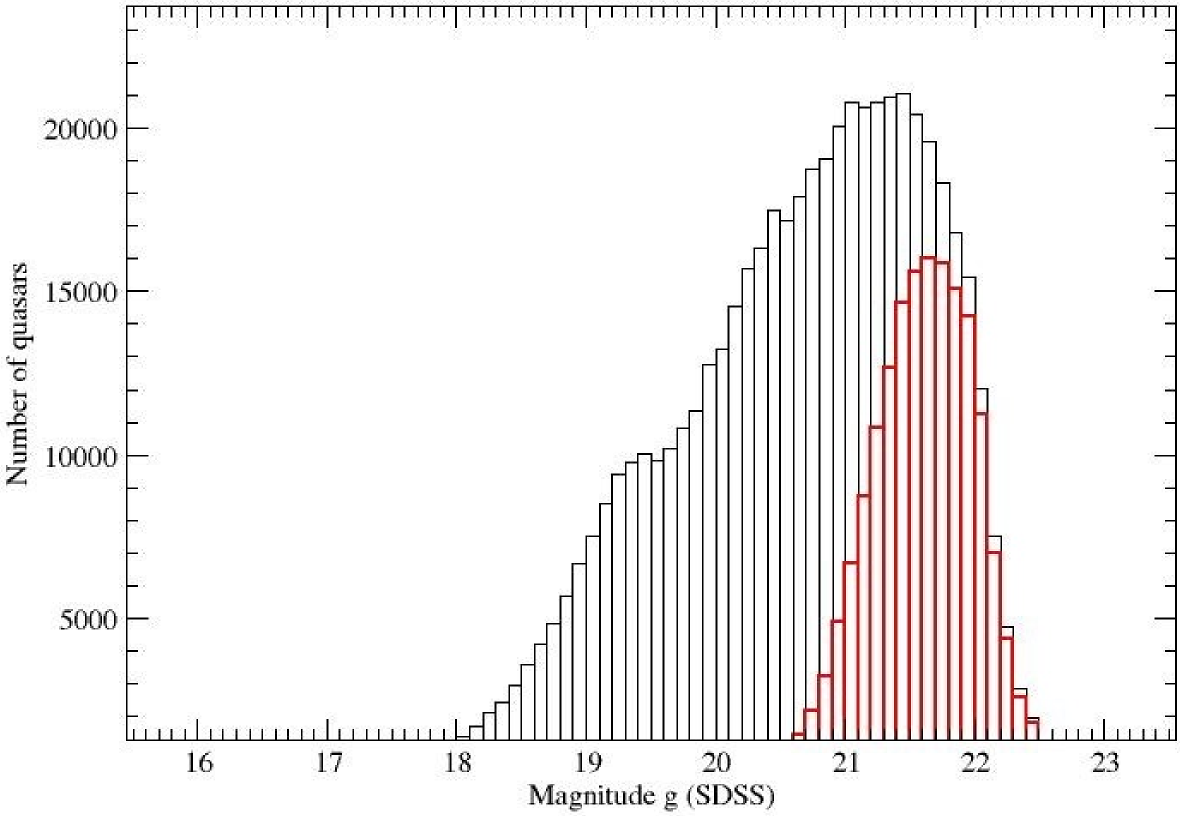

Fig. 7: *Distribution of the number of quasars per g magnitude bin, for the SDSS objects belonging to the LQAC-5 (in black). Distribution of the objects no cross-matched with Gaia DR2 (in red).*

For cross-matched objects, the correspondence between G (Gaia) and g (SDSS) gives insight in the amplitude of the discrepancy between these magnitudes, which can be due to two origins: one is the difference between the photometric systems, the other is the variability of fluxes of the objects, which can reach more than one magnitude for a limited period of time. In Fig. 8 we plot this correspondence, after using the polynomial fit between the two photometric systems established by (Jordi et al. 2010). This fit converts the initial G (Gaia) magnitude in the g (SDSS) through a polynomial transformation between the two photometric systems.

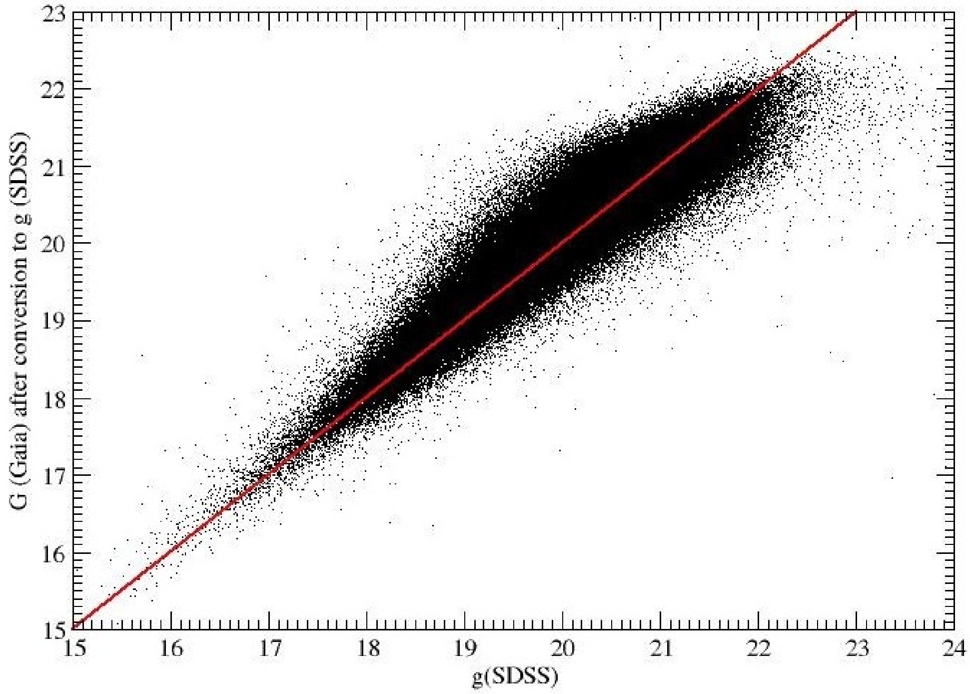

Fig. 8: *Correspondence of the g (SDSS) magnitude computed from G (Gaia) (Jordi et al. 2010) with respect to the g magnitude for SDSS quasars with a Gaia counterpart.*

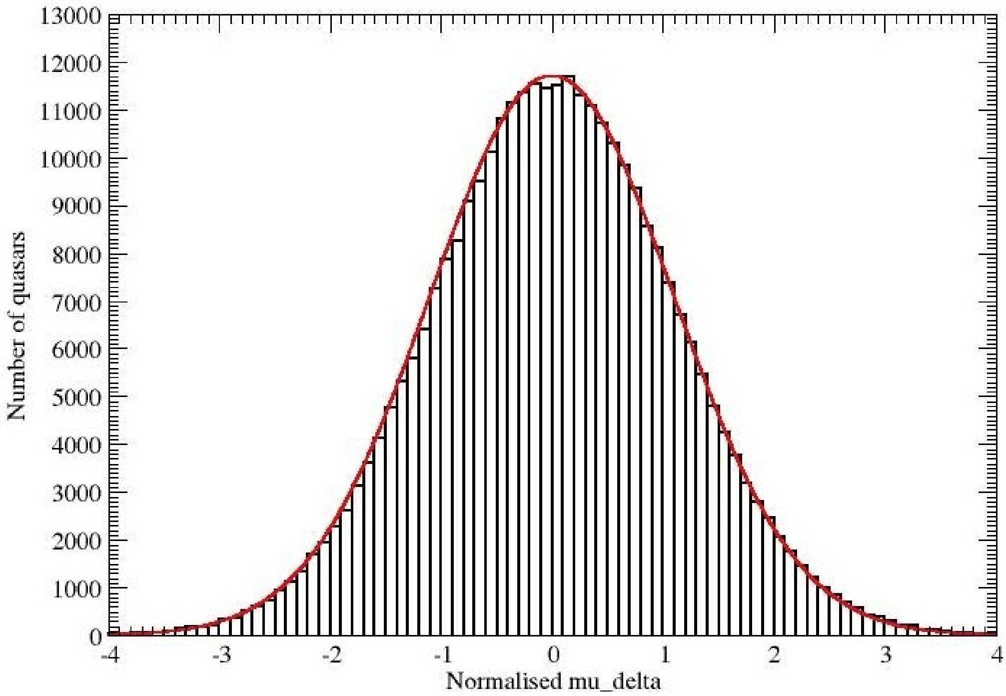

Fig. 9: *Normalized value $\mu(\delta)/\sigma_{\mu(\delta)}$ of the component of the proper motion in declination (from Gaia DR2 data) of the LQAC-5 quasars cross-identified with Gaia. The red line is a Gaussian distribution with a mean of 0 and standard deviation of 1.1.*

One of the up-to-date attractive subjects of investigation concerns the presence of quasars with a significant value of proper motion according to Gaia DR2 measurements. First, we analysed the behaviour of the normalized value μ/σ_μ of both components of proper motion in right ascension and in declination. The distribution is quasi-perfectly Gaussian for both coordinates as shown in Figure 9 in declination, thus confirming a statement already found by Mignard et al. (2018) for their CRF2 extragalactic sources. Then we analysed the distribution of the total amplitude of the proper motions, taken from the DR2 data, whose result is displayed in Figure 10. We observe a Rayleigh-like distribution with a median value around 1.5 mas/yr and with a peak at 0.5 mas/yr. Remark that a very big proportion of objects (95.4%) verify $\mu/\sigma_\mu < 2$ so that we cannot categorically conclude that they are not fixed with respect to the ICRF. On the other hand, we concentrated our study on objects with proper motion larger than 10 mas/y and with $\mu/\sigma_\mu >$ 5, which characterizes a high probability of existence of a real proper motion. Results are shown in Table 3 where 16 objects could be found satisfying the conditions above. In a second step we studied the ICRF3 quasars (Charlot et al. 2020) with proper motions larger than 1 mas/y and with $\mu/\sigma_\mu > 5$. In view of their criteria of selection from VLBI observations, the conditions above can be considered as characterizing a significant displacement of the photo-centre. Results are presented in Table 4. All these results show that searching for the astrophysical causes of significant proper motions for the objects above should be of invaluable interest.

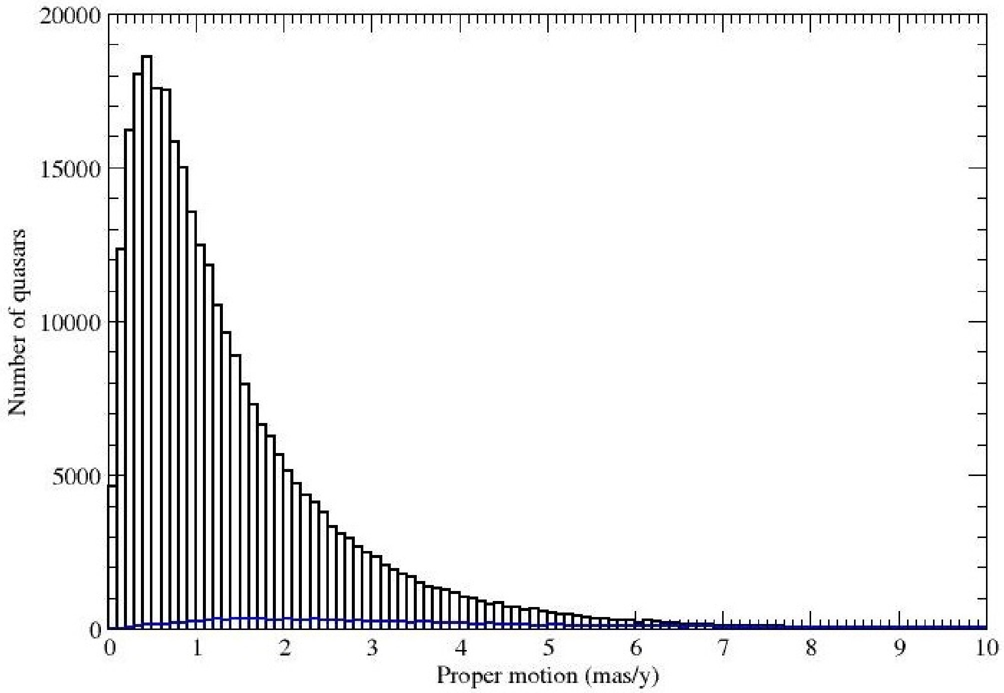

Fig. 10: *Distribution of the amplitude of proper motion for the LQAC-5 quasars cross-matched with Gaia DR2.*

Table 3: *List of the quasars of the LQAC-5 cross-matched with Gaia DR2, having a proper motion μ larger than 10 mas/yr, and satisfying the condition μ/σ_μ > 5*

α (∘)	σ_α mas	δ (∘)	σ_δ mas	$\tilde{\omega}$ mas	$\sigma_{\tilde{\omega}}$ mas	μ mas/y	σ_μ mas/y	z	G	BP	RP
8.2089013648	0.743	-10.8993572519	0.546	-5.384	0.983	22.444	2.230	2.435	19.026	18.781	18.306
16.3946967299	0.320	-27.6160917371	0.236	7.124	0.479	24.986	1.074	0.850	17.804	17.805	17.454
117.3123508035	0.517	27.1662716358	0.308	2.560	0.605	15.233	1.314	6.260	19.922	19.688	19.662
119.6010993806	0.651	14.9645671193	0.365	3.842	0.806	12.546	1.447	2.568	19.298	19.515	18.418
134.5416611091	0.616	55.1697373421	0.449	0.139	0.671	10.090	1.564	1.417	20.210	20.449	19.563
135.3152311805	0.620	-66.6093714049	0.562	0.644	0.598	12.377	1.882	0.000	20.215	20.781	18.912
139.3137082009	0.905	-2.3852827588	0.830	-0.259	1.063	20.358	3.037	1.287	19.454	19.327	18.681
235.8657942859	0.625	-1.4926802927	0.463	6.271	0.851	15.892	1.540	1.231	18.174	18.125	17.089
235.8727613597	0.064	33.9857684441	0.082	0.328	0.092	15.225	0.229	2.160	16.422	16.729	15.899
237.0639192279	0.330	28.7475575704	0.399	-0.109	0.563	10.801	1.325	2.306	20.063	20.173	19.392
237.0746243522	0.518	4.6837787907	0.432	3.170	0.637	18.969	1.514	1.034	19.309	18.952	18.267
242.1217994774	0.622	27.2740965329	0.691	1.513	0.989	14.643	2.271	2.591	20.151	20.224	19.146
249.0882074948	1.123	11.6285202879	0.799	-18.609	1.819	14.477	2.830	1.591	20.036	19.914	18.989
250.4949708516	0.120	15.4254595973	0.110	0.092	0.197	11.599	0.347	0.871	18.676	18.982	18.151
261.9937121681	0.545	56.7386750497	0.668	-1.434	0.634	14.633	1.950	1.773	19.833	19.997	19.069
359.2572207669	0.823	-2.4293386938	0.370	-1.015	0.945	17.422	1.938	0.719	19.755	20.035	18.655

Table 4: *List of ICRF3 quasars having a proper motion μ larger than 1 mas/yr, and satisfying the condition μ/σ_μ > 5.*

Name	α (∘)	σ_α mas	δ (∘)	σ_δ mas	$\tilde{\omega}$ mas	$\sigma_{\tilde{\omega}}$ mas	μ mas/y	σ_μ mas/y	z	G	BP	RP
0149+710	28.3577065085	0.314	71.2517957182	0.349	0.051	0.384	4.856	0.874	0.022	17.691	100.000	100.000
0321+467	51.3345987257	0.531	46.9185095434	0.331	0.161	0.646	7.196	1.747	0.000	19.211	18.836	17.755
0600+063	90.8096981410	0.103	6.3742787710	0.097	0.676	0.122	5.146	0.322	0.000	16.067	16.497	15.310
0603+476	91.8468957878	0.069	47.6630394728	0.064	-0.081	0.078	6.418	0.186	0.540	16.829	17.275	16.090
0620-011	95.7414266030	0.352	-1.1575327855	0.341	0.050	0.382	5.713	0.989	1.400	19.374	19.811	18.662
0757+441	120.2844842386	0.402	44.0194876510	0.292	1.442	0.622	6.680	1.064	1.072	19.653	20.051	18.879
0805-077	122.0647334850	0.165	-7.8527462146	0.093	0.084	0.173	7.282	0.398	1.837	18.269	18.637	17.471
0927-378	142.4893922167	0.069	-38.0300832649	0.081	0.404	0.112	5.371	0.211	0.000	17.767	18.327	16.997
1045-620	161.9285907721	0.232	-62.2873964223	0.196	0.207	0.263	8.582	0.543	0.000	18.879	19.309	18.068
1055+567	164.6571986351	0.032	56.4697797770	0.032	-0.072	0.050	9.337	0.100	0.143	16.181	16.323	15.438
1228+126	187.7059264664	0.525	12.3911248881	0.490	-2.816	0.666	13.405	1.502	0.004	15.794	100.000	100.000
1508-656	228.2151958153	0.315	-65.8840198033	0.385	1.318	0.557	8.918	1.015	0.000	19.651	20.280	18.516

U.S. Naval Observatory IERS ICRS Centre Activities During 2019–2020

USNO concentrated on nine primary areas of work in support of maintenance and improvement of the Celestial Reference Frame:

1. Continued support, maintenance, and improvement to the ICRF by implementing new parameters and features from the IAU-sanctioned and adopted ICRF3.
2. URAT bright stars southern hemisphere surveys
3. Development and deployment of the Deep South Telescope (DST) at Cerro Tololo Interamerican Observatory (CTIO).
4. Execution of a deep, near infrared (near-IR) survey in the northern hemisphere using the United Kingdom Infrared Telescope (UKIRT)

5. Management of ICRS/ICRF observations utilizing the Very Long Baseline Array (VLBA)

6. Determination of ICRF objects with multiple radio components.

7. Assembly of the Washington Multiple-AGN catalog for consideration in CRF work.

8. Development, jointly with Paris Observatory, of the Fundamental Reference AGN Monitoring Experiment (FRAMEx).

9. Characterization of Gaia Early Data Release 3 (Gaia EDR3).

Support, Maintenance, and Improvement to the ICRF3

USNO continued to contribute and make improvements to the global VLBI solutions throughout 2019 and 2020 in support of the ICRF. The USNO global VLBI solutions were updated and improved in a number of ways. We implemented the 303 S/X band ICRF3 defining sources into our solutions by using this list as the a priori positions for defining the axes of the reference frame. These 303 defining sources differed from the previous 295 defining sources from the ICRF2 that we used prior to 2019, by their more isotropic distribution over the celestial sphere.

In addition, we changed the reference epoch in accordance with the ICRF3 recommendations to 2015.01.01, thus updating the nearly 20-year-old epoch 2000.01.01, used prior to 2019. We included a Galactic aberration term equal to 5.8 μas/yr in order to correct for the amplitude of the solar system barycenter acceleration vector (see Fig. 3, Charlot et al. 2020). Finally, the last improvement that USNO made in its global VLBI solutions was the utilization of the Vienna mapping function (VMF1) instead of the neo-mapping function used prior to 2019 for improved calibrations of the troposphere. Together, these updates facilitated all of the USNO IVS Analysis Center data products, such as the daily intensive observations and individual rapid 24-hour sessions, to be in agreement with the ICRF3.

We compared the difference between the USNO 2018 VLBI global solution (usn2018b) and the USNO 2019 solution (usn2019c) in order to assess how the changes affected the five Earth Orientation Parameters (EOPs). Figure 11 shows the results of this analysis and we find good agreement between the 2018 and the 2019 solutions.

In addition to implementing updates to the USNO VLBI global solution, USNO also began contributing to the ITRF2020 by submitting SINEX files to be used in the final solution. These activities are ongoing and USNO is planning to submit a final set of SINEX files in time for the ITRF2020 solution, which is expected to be released in mid-2021.

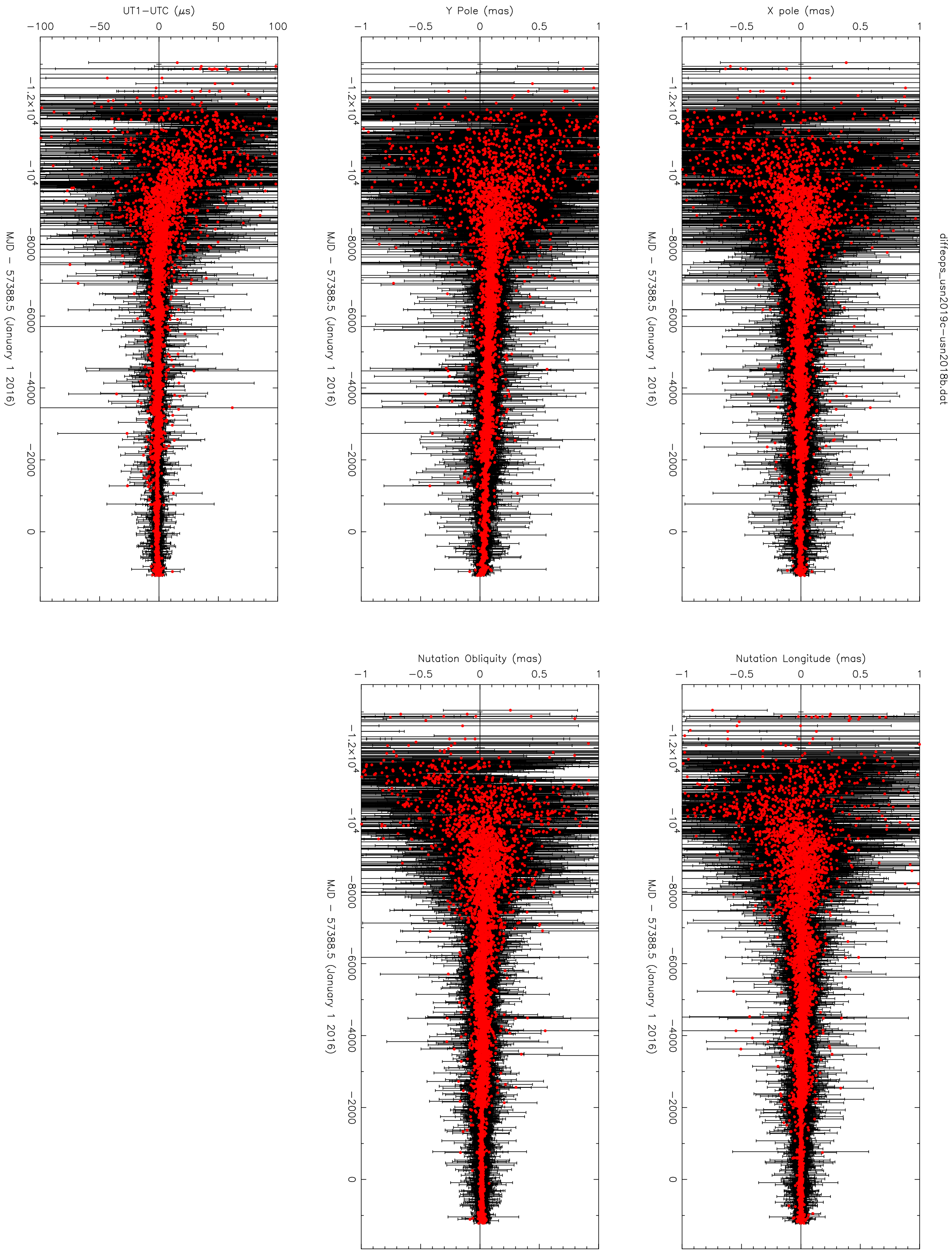

Fig. 11: *The difference between the 2018 and 2019 VLBI global solutions for each of the five EOPs.*

URAT Southern Hemisphere Bright Star Survey

While the core of optical astrometric data for the next few decades is expected to come from the Gaia mission (Mignard et al. 2018), there are limitations with Gaia. Specifically, the Gaia focal plane physically saturates at G=12 in regular observing mode. The second Gaia data release (April 2018) contains astrometric results for some stars in the 3.5 to 6 magnitude range, observed with special “bright star modes”. As summarized in Brown et al. (2020), bright star astrometry in Gaia Early Data Release 3 (EDR3) is improved somewhat over DR2, with uncertainties in positions and parallaxes respectively reduced to 0.43 and 0.27 of their DR2 values, although Gaia EDR3 is similarly incomplete at the bright end.

In order to address this gap in the optical reference frame, USNO is producing the UBSC (USNO Bright Star Catalog), which is based on UBAD, URAT and Hipparcos data. UBAD is an observational program in the northern hemisphere using the 1.55m Strand Reflector at the Naval Observatory Flagstaff Station (NOFS). A preliminary UBAD catalog of over 340 stars of magnitude 3 and brighter was generated. The USNO Robotic Astrometric Telescope (URAT) observational program run for 2.7 years at Cerro Tololo Interamerican Observatory (CTIO) to cover the southern sky. For the UBSC data of about 1200 stars of magnitude 4.5 and brighter were used. The intermediate level Hipparcos data are used as early epoch to allow a rigorous solution of all 5 astrometric parameters. More UBAD observations were performed in 2020 to conclude this observational program. Reductions of UBSC are in progress, and construction of a final catalog is expected in 2021.

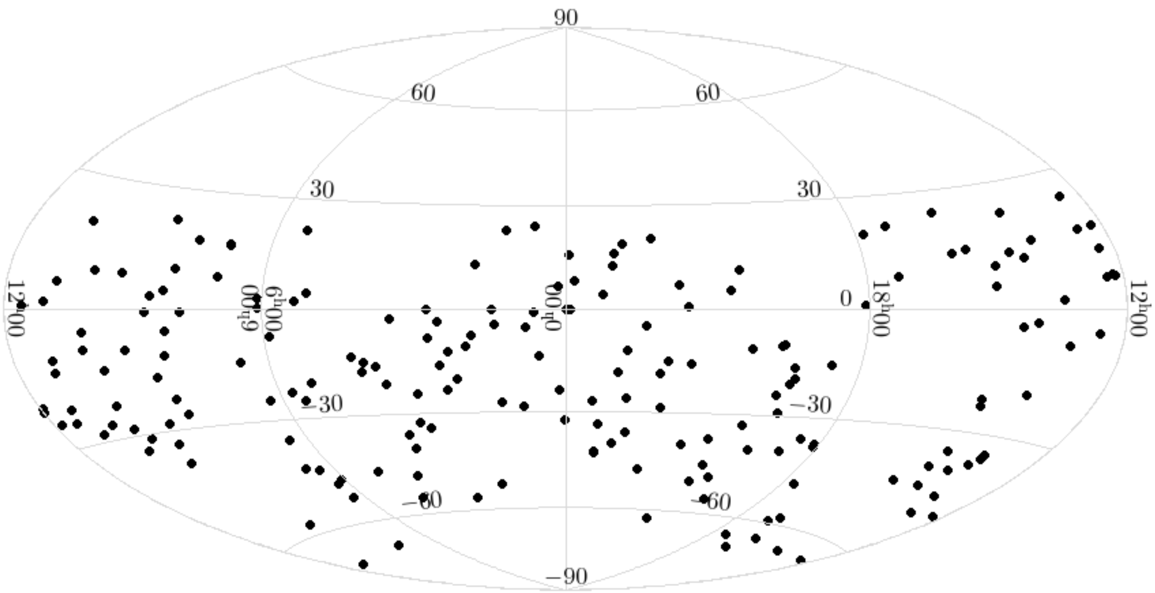

Fig. 12: *Aitoff projection of the 2019–2020 DST target list, which is comprised of 199 objects.*

Deep South Telescope (DST)

About 10% of ICRF sources display abnormally large optical vs. radio position differences when comparing Gaia results with VLBI data. In order to investigate this further, USNO acquired a new 1-meter telescope from PlaneWave Instruments in 2018. This Deep South Telescope (DST) was deployed at CTIO in Chile in March 2019. A 4k Sophia CCD camera was ordered from Princeton Instruments. A mishap during shipment of the camera and other instrumental issues caused a delay of several months. Survey observations with DST began in August 2019 with a target list of about 200 extragalactic sources, shown in Figure 12. Observing at CTIO continued until shutdown due to pandemic in April 2020. Over 12,000 on-sky exposures were obtained with about 6,300 of sufficient quality to pass astrometric reductions. An investigation into systematic errors lead to various calibrations of the data and to preliminary position results for over 150 targets. In November 2020 DST observations resumed, however, a camera problem was discovered. Various instrumental issues need to be fixed before reaching full operations capabilities. This program is part of the joint USNO/OP collaboration (FRAMEx, see below for more information). We show images of the DST from 2019 in Figure 13.

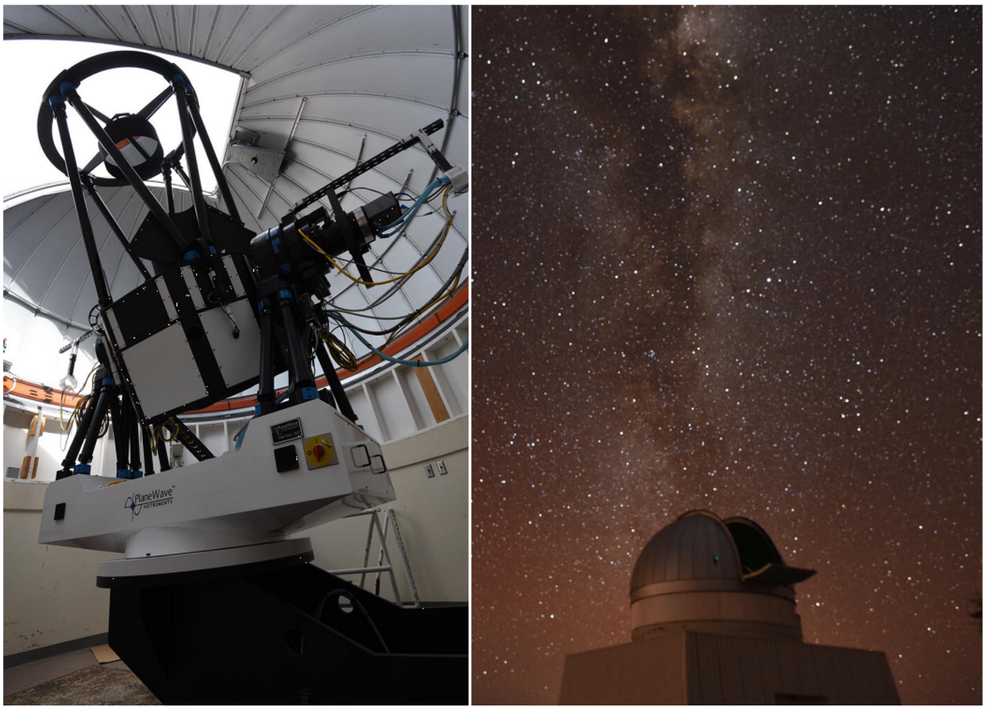

Fig. 13: *Left: DST at CTIO, 2019. Right: DST night operations, 2019.*

USNO UKIRT Hemispherical Survey

USNO, in collaboration with the Institute for Astronomy (IfA) at the University of Hawaii (UH); the School of Physics and Astronomy, Nottingham University; Institute of Astronomy, University of Cambridge; and the Institute for Astronomy, University of Edinburgh, continued a K-band

(2.2 μm) multi-year, northern hemisphere survey in the near-IR using the United Kingdom Infrared Telescope (UKIRT). This survey is targeted for completion in the 2021 timeframe. When completed, the K-band survey will provide a catalog to fainter than 18th magnitude that complements the VISTA Hemisphere Survey in the southern hemisphere (McMahon 2013). A similar multi-year UKIRT survey in H-band (1.6 μm) to fainter than 19th magnitude has been initiated with completion expected during 2022. When combined with the J-band (1.2 μm) UKIRT survey (Dye 2018), the K- and H-band data will provide deep photometric and astrometric data for the three standard NIR astronomical photometry bands. Figure 14 shows the progress of the K and H-band surveys through November 2020. Approximately 90% of the K-band and 10% of the H-band data have currently been obtained. When combined with earlier surveys, 100% of the northern sky between declinations 0 and +60 deg will have been covered to unprecedented depths and astrometric accuracy.

ICRS/ICRF Observations with the Very Long Baseline Array (VLBA)

USNO sponsored multiple 24-hour astrometric/geodetic-style observations on the VLBA at S/X bands and K-band through the USNO 50% Timeshare Agreement on the VLBA. These sessions were optimized for imaging by ensuring adequate on-source integration time and uv coverage for each ICRF target observed such that high fidelity images could be produced in addition to astrometric measurements. In 2019, USNO provided the time for 19 sessions at S/X as part of the UG002 series and 13 sessions at K-band as part of the UD001 series where each 24-hour session contained approximately 250 ICRF sources. The S/X observations increased the number of observations for ~3500 individual sources for improving the astrometry of the ICRF. In 2019, USNO also sponsored an IVS series of six 24-hour sessions known as the CN-series, which were executed simultaneously to the IVS R1 rapid sessions such that systematic errors in the astrometry and EOPs could be determined. USNO also sponsored six Research and Development with the VLBA (RDV) sessions, which combine the VLBA array with a handful of IVS stations for the purposes of imaging and monitoring faint ICRF sources. The RDV series is in collaboration with Bordeaux Observatory and the data are used for producing all of the images that comprise the Bordeaux VLBI Image Database (BVID).

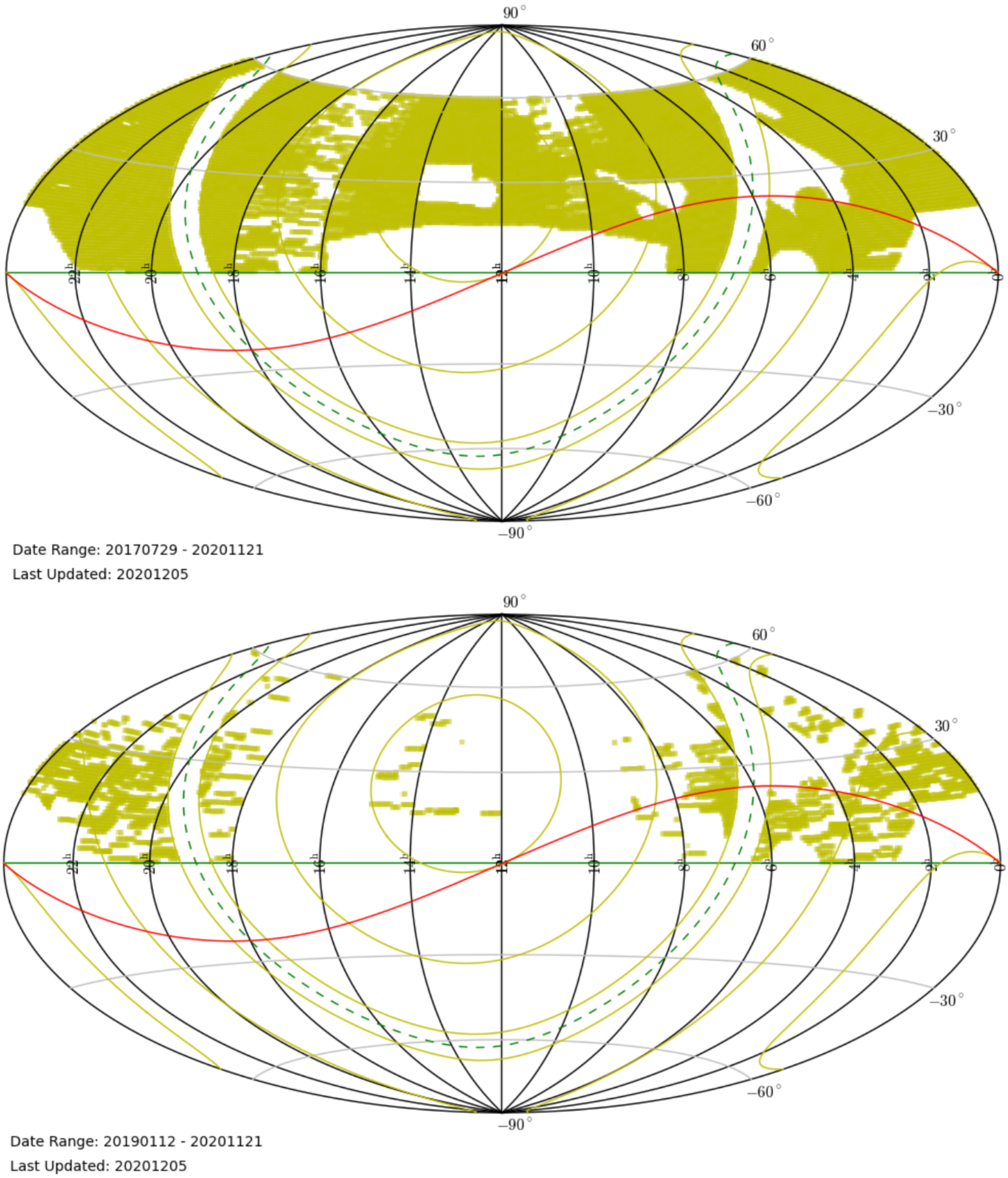

Fig. 14: *Top: UKIRT K-band survey progress, as of November 2020. Note that the galactic plane and the region centered around the North Galactic Pole (RA 12 h 510, DEC +27 deg 070) were previously surveyed; the current survey fills in the gaps. Also note that UKIRT cannot observe above DEC +60 deg; this “polar cap” will be filled in with dedicated observations using a different telescope at a later time. Bottom: H-band survey progress, as of November 2020.*

In 2020, USNO continued to sponsor ICRF 24-hour astrometric and geodetic observations on the VLBA through the USNO-VLBA 50% time-share allocation agreement. In 2020, USNO provided the time for 6 RDV sessions, 12 K-band sessions, and 12 S/X-band sessions. Beginning in August 2020, the K-band and S/X-band sessions were aligned in time such that they were run back-to-back in a pseudo-simultaneous manner. The source lists between the K and S/X bands were also matched. These alignments allow for monitoring and studying ICRF quasars in the radio at three frequencies in a quasi-simultaneous fashion for the purposes of understanding flux and/or astrometric variability and source structure so that we can better understand the nature of the emission and perhaps form predictions for when sources might become problematic.

USNO began creation of its own image data archive called the Fundamental Reference Image Data Archive (FRIDA) which will be hosted on the new USNO website scheduled for debut in 2021. Initially, the observations that will contribute the majority of the images that will be available on FRIDA come from the VLBA-only sessions as these are the sessions through which development of a calibration and imaging pipeline using the NRAO Common Astronomy Software Applications (CASA) package has been accomplished. FRIDA will be an interactive web interface for users to obtain access to USNO's data archive containing all of the radio images created with data from the VLBA. USNO intends to host calibrated images in FITS format as well as provide the calibrated uv datasets and ancillary information including plots showing the amplitude versus uv distance and uv sky coverage as diagnostic tools of the data quality for each image. Users will be able to download all of the data made available through FRIDA. Eventually, USNO plans to host all of the K-band images from the UD001 series as well as the RDV data. In addition, USNO will host all ancillary archival data that were previously part of the Radio Reference Frame Image Database (RRFID) which span frequencies from S/X, K, and Q-bands for a number of ICRF sources. Figure 15 gives a series of example images that will be hosted on FRIDA.

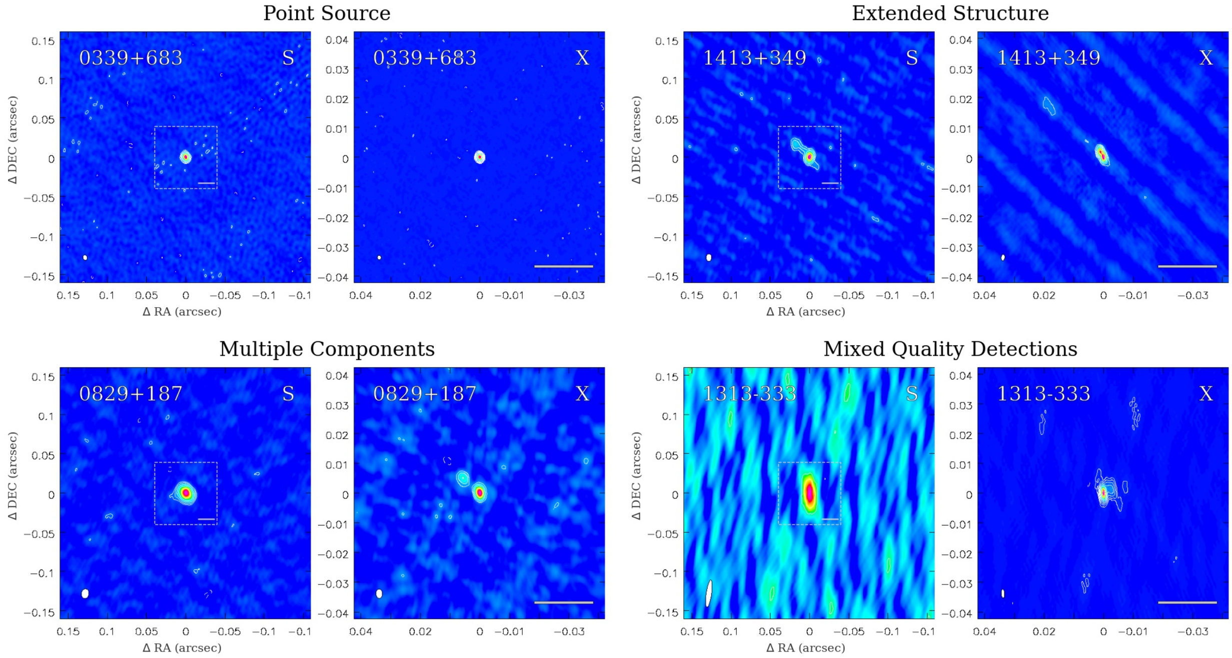

Fig. 15: *S-band (left) and X-band (right) images showing a sample of sources from the ICRF that will be available on FRIDA. The white dashed box in the S-band images denotes the size of the X-band images. The restoring synthesized beam is shown in the bottom left corners, and the angular scale bars are 20 mas.*

ICRF Objects with Multiple Radio Components

USNO has produced VLBA images of ~3500 out of 4536 S/X ICRF3 sources above a declination limit of -45°, to be described in Hunt et al. (2021, in preparation), and made available through FRIDA. In brief, the VLBA S/X dual frequency system provided astrometric measurements similar to that of the IVS S/X observations and comprise the majority (68%) of ICRF3 data (Charlot et al. 2020). Twelve 32-MHz channels were used in X-band (8.6 GHz) and four 32-MHz channels were used in S-band (2.3 GHz), the latter of which is used for astrometric calibration of the ionosphere. Integration times were ~60 to ~160 seconds for target sources and ~24 seconds for defining sources that were used to tie the astrometric results to the ICRF. Images were produced at both S- and X-bands.

We visually classified the ICRF source images in order to select those with multiple sources, which may pose an issue for the link to Gaia-CRF. For example, a heavily reddened quasar with a collimated jet may suffer from a large optical-radio offset, as the Gaia counterpart will be centered on the jet, missing the location of the radio core. If the system is a dual supermassive black hole (SMBH) quasar, predicted from hierarchical cosmological simulations to be common, then it is possible that the Gaia optical counterpart does not in fact correspond to the ICRF source but rather its neighbor. While strong optical emission from the accretion disk of an AGN is ubiquitous, only about 15–20% of quasars are “radio-loud”, meaning that their radio emission dominates over their optical emission

(Kellermann et al. 1989). As the ICRF quasars are selected to be radio sources, this means that they are more likely to be radio-loud, and any neighboring AGN may well be much less luminous in the radio. If the neighboring AGN's optical emission becomes a significant fraction of the ICRF quasar's optical emission, be it from intrinsic luminosity variability or variable reddening, then the ICRF quasar will exhibit an optical-radio offset. Note also that differential luminosity variability is likely to be the true cause of astrometric jitter even in true, unresolved, binary (gravitationally-bound) systems. At the astrometric limit of ICRF3, ~30 μas, even a 10^9 solar mass black hole binary system at z = 1 will have an orbital period of ~100 yr (Figure 16).

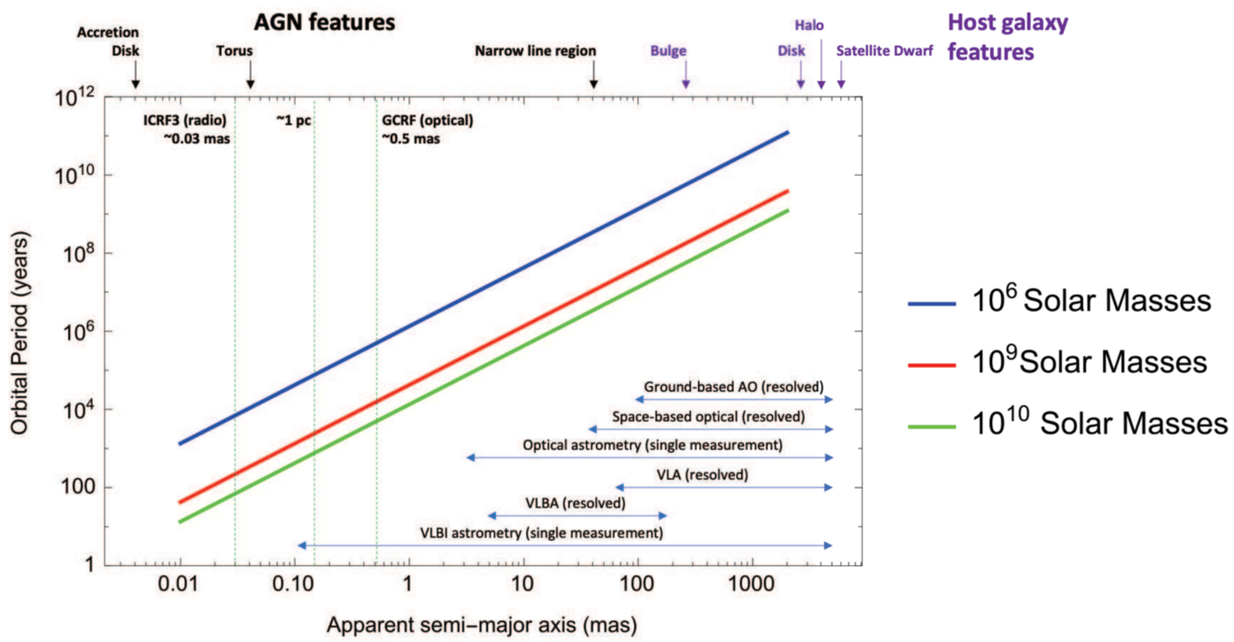

Fig. 16: *Angular separation versus orbital period for a z = 1 binary black hole system (from Dorland et al. 2020).*

To flag images with potential multi-sources, we used SExtractor (Bertin & Arnouts 1996). This produced a list of 143 images of 110 unique ICRF objects. The three study leads (N. Secrest, J. Frouard, and L. Hunt) independently classified each image in terms of the number of compact components (Nc), defined as components consistent with the synthesized beam of the observation, and extended components (Ne), defined as those components with additional structure inconsistent with the synthesized beam. For objects not agreed upon in the first round of classification, a second round of classification was done, without knowledge of how the objects were first classified. After this second round, remaining disagreements were jointly classified by all three investigators. The point during the process that consensus was reached will be used to estimate the reliability of classification. Additional information on the reliability (and completeness) of this method will be obtained by comparing with images of multi-source objects not initially flagged for inspection, and morphological differences between this analysis and images available on the Bordeaux VLBI Image Database will be noted. The multi-source classifications, along with reliability and completeness estimates, will be published as a catalog in the 2021 timeframe, likely as an ApJS owing to broad interest in these sources from the wider astronomical community. We show some examples of our classifications in Figure 17.

The Washington Multiple-AGN Catalog

As explained above, knowledge of whether or not an ICRF object is a dual or binary AGN may prove essential to flagging likely "pathological" sources with large optical-radio offsets, thereby helping to refine the optical-radio CRF link. Towards this goal, in 2020, USNO started developing the Washington Multiple-AGN Catalog (WMAGN), its name being a nod to the venerable Washington Double Star Catalog maintained by USNO (e.g., Mason et al. 2001). The current goal of this catalog is to concatenate all confirmed and candidate dual and binary AGNs in the literature into a single catalog, for future use when considering optical-radio offsets and CRF link sources, as well as to be of use to the wider astronomical community.

The WMAGN catalog, version 0.1, was completed in the fall of 2020. It was assembled over the summer by GMU PhD candidate R. Pfeifle, whose PhD thesis is on dual and multiple AGNs, as part of an ongoing USNO-GMU collaboration. WMAGN version 0.1 contains 422 unique multiple AGN systems, 18 of which are ICRF3 sources. Of these 18, 11 are confirmed or candidate binary AGNs. The catalog is estimated to be 90 – 95% complete up to 2010. Once it is complete up to 2020 and undergoes some additional quality control tests, USNO intends to publish it, likely in ApJS. In the long term, the catalog will be updated on a yearly basis. The current WMAGN data model is shown in Table 5.

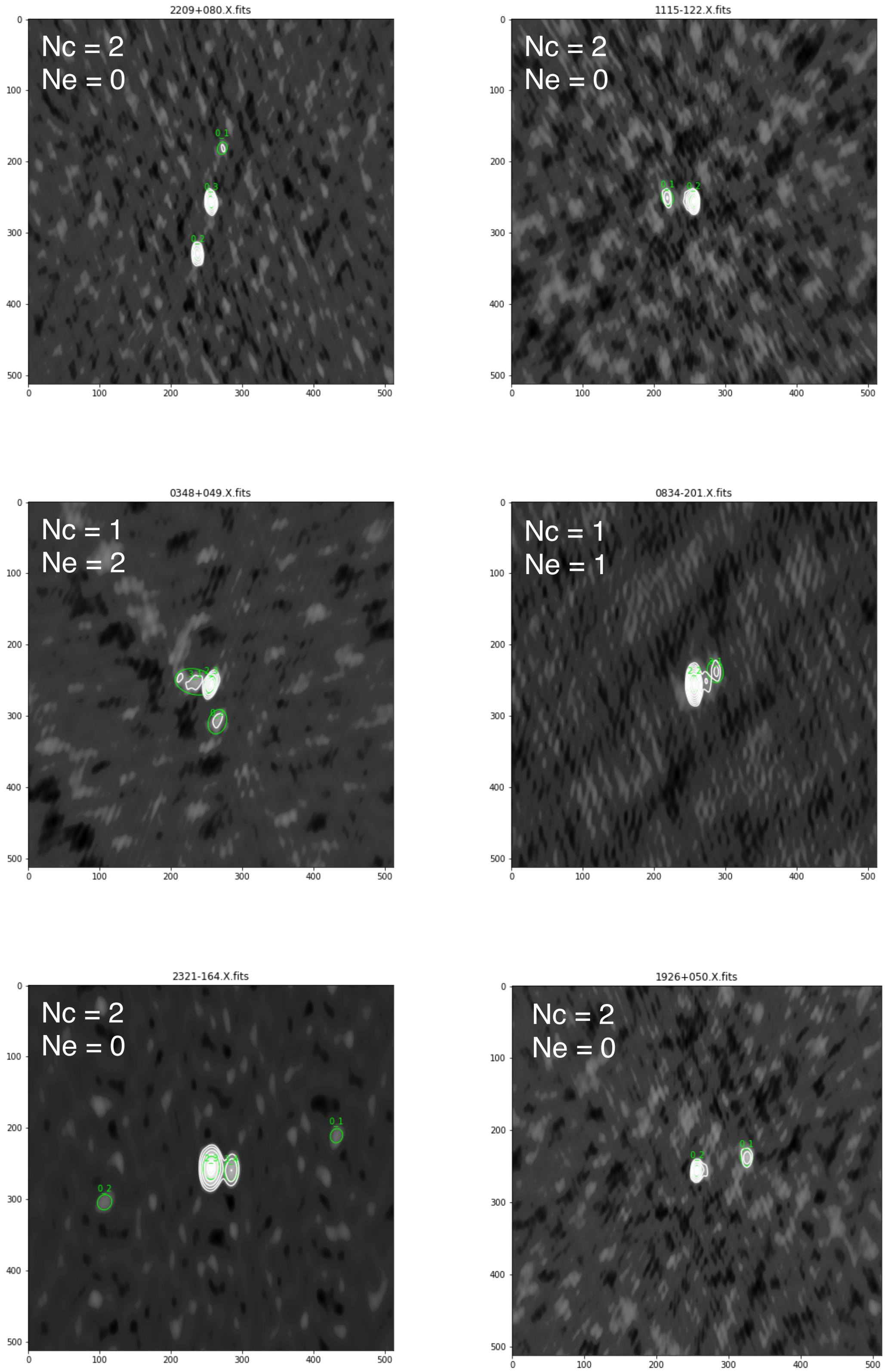

Fig. 17: *Example VLBA X-band images of ICRF objects with multiple sources, either resolved (Ne), or compact (Nc).*

Table 5: *WMAGN version 0.1 data model.*

index	Unique internal system identifier
System Type	Type of multiple AGN (e.g., dual AGN)
Literature Name	Identifier used in literature source
Name	Used name
Selection Method	Criterion used to identify multiple AGN system
Confirmation Method	Criterion used to confirm multiple AGN system (do not use in v0.1)
z	Redshift
z_type	Spectroscopic or photometric
RA	Right Ascension
Dec	Declination
RA_deg	Right Ascension in degrees
Dec_deg	Declination in degrees
Equinox	RA/Dec equinox (always J2000)
Coordinate_waveband	Wavelength/passband of RA and Dec
Coordinate_Source	Source of RA and Dec
Brightness	Apparent magnitude
Brightness_band	Passband of apparent magnitude (e.g., V, SDSS g, 1.4 GHz NVSS)
Brightness_type	(e.g., mag, asinh mag, mJy)
Sep	Angular separation of multiple AGNs, in arcsec
Sep(kpc)	Projected physical separation of multiple AGNs
delta_z	Difference in redshifts between multiple AGNs
dV	delta_z times the speed of light in km/s
Paper(s)	System source literature
BibCode(s)	NASA ADS bibliography code for Paper(s)
DOI(s)	URL of Paper(s)
Notes	Salient peculiars or caveats for system

Fundamental Reference Frame AGN Monitoring Experiment (FRAMEx)

The Fundamental Reference AGN Monitoring Experiment (FRAMEx) was conceived at a May 2018 USNO-Paris Observatory IERS ICRS Centre meeting. The purpose of FRAMEx is to study representative samples of AGN/quasars to understand the physical processes potentially involved in optical-radio positional offsets seen in many ICRF sources. We defined two samples for study: a volume-complete sample of local AGN and a sample of quasars with significant optical-radio (Gaia-VLBI) positional offsets. Photometric observations of the latter sample, which are being taken with the new USNO Deep South Telescope (DST; PI: Zacharias, see above) are currently being analyzed.

The details of the volume-limited sample target selection were provided in IERS Annual Report 2018, but here we provide the salient findings since that report:

- Despite all of the hard X-ray (14 – 195 keV) selected AGNs in the local volume being detected with the VLA, only 9 out of 25 (36%) AGNs were detected with the VLBA, indicating that the "core" radio emission from these AGNs is being resolved-out on mas scales.
- Including both detections and upper limits, AGNs systematically "jump out of the plane" of the "Fundamental Plane" of black hole accretion (e.g., Merloni et al. 2003) when using high-resolution VLBA data, despite being consistent with the Fundamental Plane for lower-resolution VLA data. See Figure 18, taken from FRAMEx paper I (Fischer et al. 2020).
- The L_R / L_X ratios of our detections are between 10^{-7} – 10^{-4}, roughly in line with expectations from coronal synchrotron emission (L_R / L_X ~10^{-5}; Laor & Behar 2008). However, given the sensitivity of our observations to L_R / L_X ratios as low as 10^{-7}, our findings raise the possibility of truly radio-silent AGNs.
- The only object in our sample that does not exhibit this jump is NGC 1052, which is an ICRF object (IERS B0238-084). It has an L_R / L_X ratio of ~10^{-2}, in line with the radio-loud / radio-quiet demarcation of L_R / L_X = 10-4.5 from Terashima & Wilson (2003).

These findings are consistent with a bimodality in radio loudness amongst AGNs. This being the case, the volume-complete AGN sample is of less utility for studying accretion physics relevant to ICRF quasars. However, we have continued to monitor these objects, and several projects are being carried out with USNO and its partner institutions.

Characterization of Gaia EDR3

Gaia EDR3 was released 3 December 2020, allowing for some exploration of the properties of EDR3 matches to the ICRF3, compared with Gaia DR2. ICRF3 was matched with a tolerance of 1" to Gaia DR2 and EDR3, producing a list of 3384 matches (74.6%). The overall distribution of optical-radio offsets between Gaia and ICRF3 is somewhat better, with a median value of 0.56 mas for EDR3, vs. 0.67 for DR2 (Figure 19).

The values of uncertainty-normalized offsets are similar between DR2 and EDR3 (Figure 20). For both catalogs, the normalized offsets are not consistent with expectations for offsets due to errors, providing that the formal uncertainties are accurate. The similarity in the distribution between Gaia EDR3 and DR2 is consistent with these offsets, which have been the subject of much study, being physically significant.

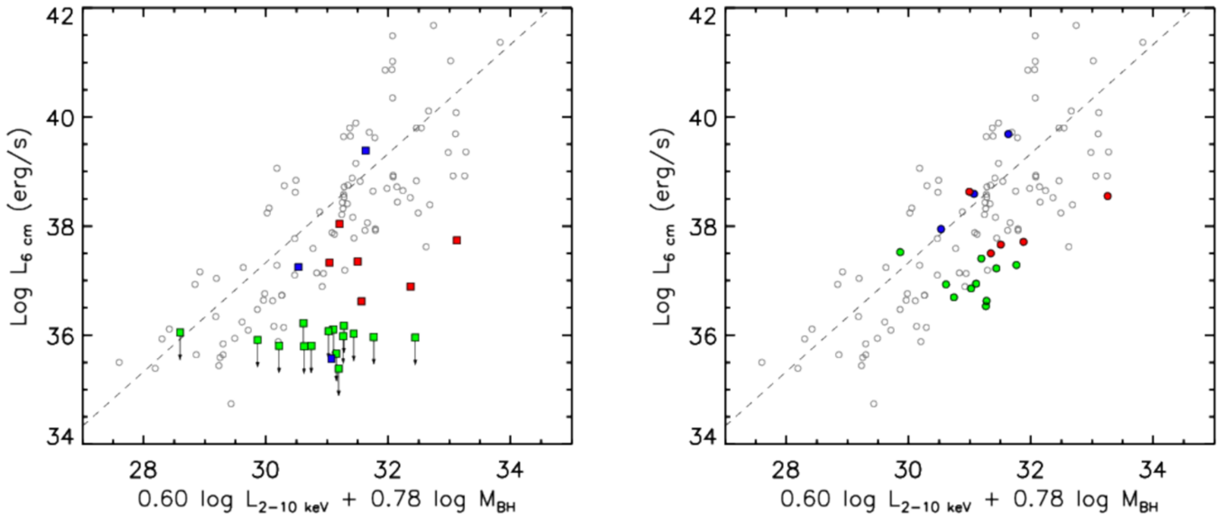

Fig. 18: *Left: fundamental plane (projected along X-ray and black hole mass axis) versus C-band luminosity for VLBA-detected AGNs and upper limits. Right: for VLA-detected objects. From FRAMEx paper I (Fischer et al. 2020).*

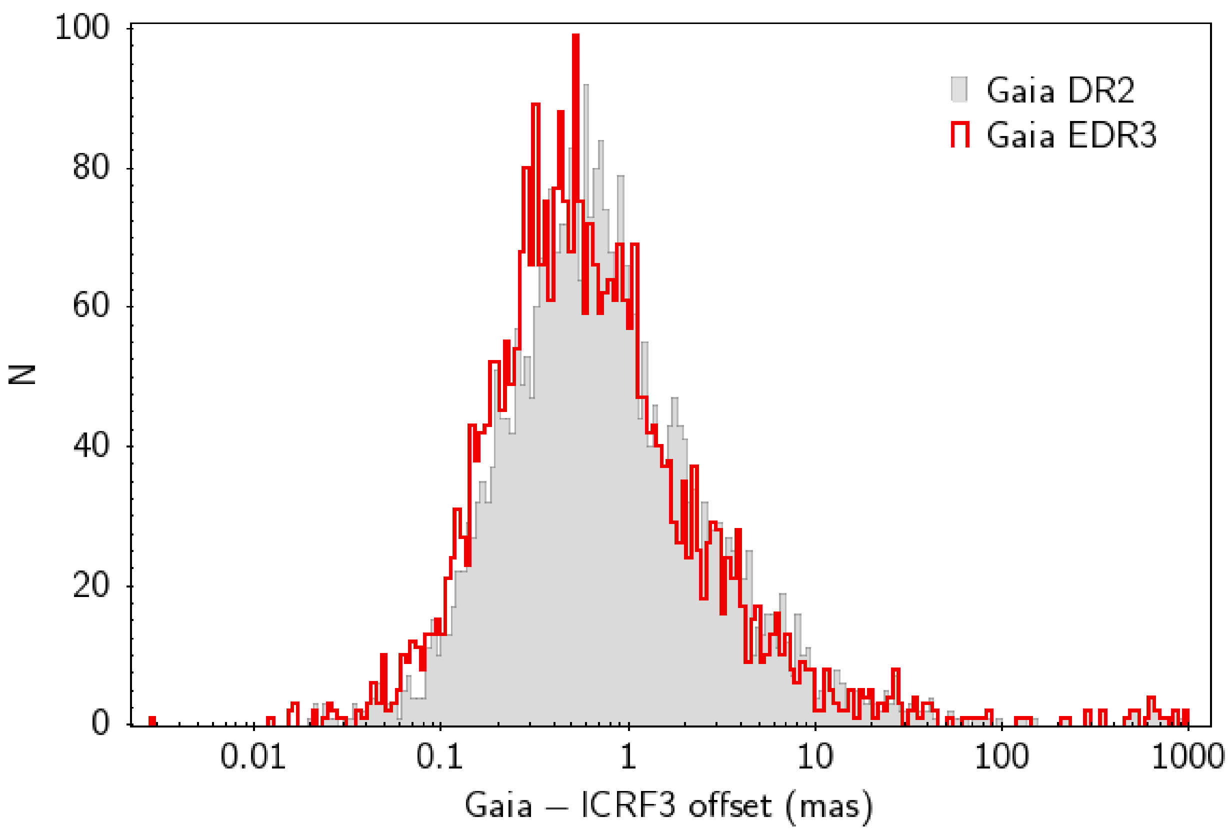

Fig. 19: *Offsets between Gaia and ICRF3 for DR2 (gray shaded) and EDR3 (red line).*

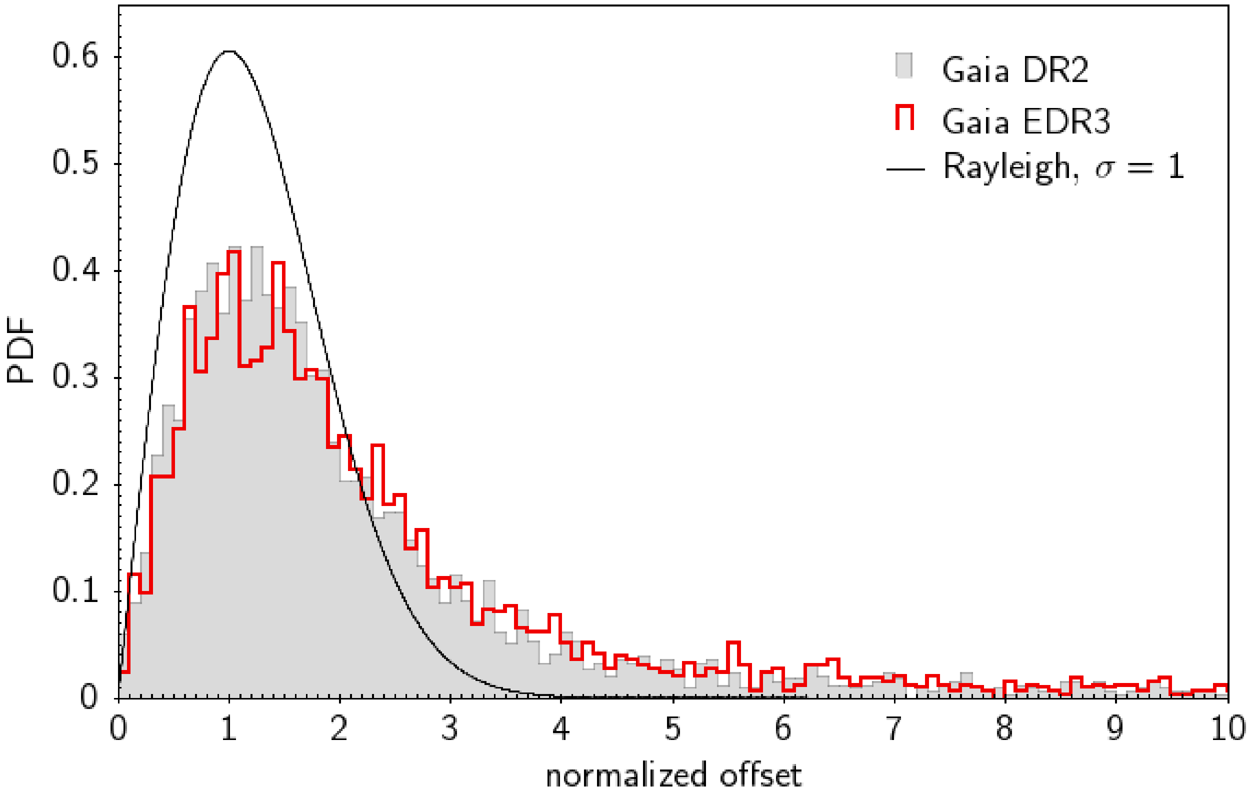

Fig. 20: *Uncertainty-normalized offsets. A Rayleigh distribution with sigma = 1 is expected if the coordinate errors are normally-distributed with errors corresponding to their formal errors (see, e.g., Makarov et al. 2019).*

Note, however, that there is some variance in the offset significance for any given source in EDR3 vs. DR2. To quantify this, we made a table of the number of sources in DR2 and EDR3 meeting varying cuts on normalized offset (X_cut; Table 6). For all thresholds, the number of sources in EDR3 is equal to or lower than those in DR2, suggesting that, overall, there are fewer objects in EDR3 with significant optical-radio offsets, although this change is small, of order a few percent. Above a normalized offset cut of 5, the two catalogs are in agreement to within 2%, suggesting that 5 is a good cut for a reliable sample of significant optical-radio offsets.

Analysis of the newly published Gaia EDR3 and ICRF3 data, as well as ongoing FRAMEx observations, is expected to produce significant new results of direct relevance to improving the evolving ICRF and its associated optical counterpart, the GCRF.

Table 6: *The number of objects in Gaia DR2 and EDR3 meeting some normalized offset threshold X_cut. Percent gives these numbers as a portion of the total catalog (3384 sources). Percent_change = N_diff / N_DR2 * 100.*

X_cut	N_DR2	Percent	N_DR2_EDR3	Percent	N_diff	Percent_change
3	778	23	709	21	-69	-9
4	538	16	516	15	-22	-4
5	415	12	406	12	-9	-2
6	349	10	340	10	-9	-3
7	291	9	289	9	-2	-1
8	254	8	252	7	-2	-1
9	221	7	218	6	-3	-1
10	198	6	194	6	-4	-2
11	175	5	174	5	-1	-1
12	158	5	158	5	0	0
13	140	4	140	4	0	0
14	126	4	125	4	-1	-1
15	120	4	120	4	0	0
16	115	3	114	3	-1	-1
17	105	3	104	3	-1	-1
18	99	3	99	3	0	0
19	88	3	88	3	0	0
20	86	3	86	3	0	0

References

Bertin, E. & Arnouts, S. 1996, A&AS, 117, 393

Charlot, P., Jacobs, C.S., Gordon, D., et al. 2020, A&A, 644, A159

Dorland, B., Secrest, N., Johnson, M., et al. 2020, Astrometry, Earth Rotation, and Reference Systems in the GAIA era, 165

Dye, S., Lawrence, A., Read, M. A., et al. 2018, The UKIRT Hemisphere Survey: definition and J-band data release, Monthly Notices of the Royal Astronomical Society, 473, 5113–5125

Fey, A.L., Gordon, D., Jacobs, C.S., et al. 2015, AJ, 150, 58

Fischer, T. C., Secrest, N. J., Johnson, M. C., et al. 2020, ApJ, accepted for publication.

Gaia Collaboration, Brown, A.G.A., Vallenari, A., et al. 2016, A&A, 595, A2

Gaia Collaboration, Brown, A.G.A., Vallenari, A., et al. 2018, A&A, 616, A1

Gaia Collaboration, Mignard, F., Klioner, S.A., et al. 2018, A&A, 616, A14

Gaia Collaboration, Prusti, T., de Bruijne, J.H.J., et al. 2016, A&A, 595, A1

Gattano, C., Andrei, A.H., Coelho, B., Souchay, J., Barache, C. and Taris, F. 2018, A&A, 614, 140

International Astronomical Union. Transactions IAU, Vol. XXXB, Proc. of the XXX IAU General Assembly, August 2018 (Ed. Teresa Lago), 2019.

Jordi, C., Gebran, M., Carrasco, J.M., et al. 2010, A&A, 523, A48

Kellermann, K.I., Sramek, R., Schmidt, M., et al. 1989, AJ, 98, 1195

Kovalevsky, J. 2003, A&A, 404, 743

Lambert, S. 2014, A&A, 570, A108

Laor, A. & Behar, E. 2008, MNRAS, 390, 847

Ma, C., Clark, T.A., Ryan, J.W., et al. 1986, AJ, 92, 1020

Mason, B., Wycoff, G.L., Hartkopf, W.I., et al. 2001, AJ, 122, 3466

MacMillan, D.S., Fey, A., Gipson, J.M., et al. 2019, A&A, 630, A93

McMullin, J. P., Waters, B., Schiebel, D., Young, W., & Golap, K. 2007, in ASPCS, Vol. 376, Astronomical Data Analysis Software and Systems XVI, ed. R. A. Shaw, F. Hill, & D. J. Bell, 127

Merloni, A., Heinz, S., & di Matteo, T. 2003, MNRAS, 345, 1057

Mignard, F. & Klioner, S. 2012, A&A, 547, A59

Pâris, I., Petitjean, P., Aubourg, E., et al. 2018, A&A, 613, A51

Souchay, J., Andrei, A.H, Barache, C., et al. 2015, A&A, 583, A75

Souchay, J., Gattano, C., Andrei, A.H., et al. 2019, A&A, 624, A145

Terashima, Y. & Wilson, A.S. 2003, ApJ, 583, 145

Titov, O., Tesmer, V., & Boehm, J. 2004, International VLBI Service for Geodesy and Astrometry 2004 General Meeting Proceedings, 267

Titov, O., Lambert, S.B., & Gontier, A.-M. 2011, A&A, 529, A91

Wright, E. L., Eisenhardt, P. R. M., Mainzer, A. K., et al. 2010, AJ, 140, 1868

Bryan Dorland, Jean Souchay, Alexandre Andrei, E. Felicitas Arias, Christophe Barache, Sébastien Bouquillon, Alan Fey, César Gattano, Sébastien Lambert, Nathan Secrest, François Taris, Norbert Zacharias